Developmental effects of oxytocin neurons on social affiliation and processing of social information

Ana Rita Nunes[1,2,*], Michael Gliksberg[2,*], Susana A.M. Varela[1,3], Magda Teles[1], Einav Wircer[2], Janna Blechman[2], Giovanni Petri[4], Gil Levkowitz[2,#], Rui F. Oliveira[1,3,5,#]

* These authors contributed equally to the work

Integrative Behavioural Biology Lab[1], Instituto Gulbenkian de Ciência, Oeiras 2780-156, Portugal.

Department of Molecular Cell Biology[2], Weizmann Institute of Science, Rehovot 7610001, Israel.

ISPA- Instituto Universitário[3], Lisboa 1149-041, Portugal

ISI Foundation & ISI Global Science Foundation[4], 10126 Torino, Italy

Champalimaud Research[5], Champalimaud Centre for the Unknown, 1400-038 Lisbon, Portugal.

Correspondence should be addressed to

G.L. gil.levkowitz@weizmann.ac.il

R.F.O. ruiol@ispa.pt

KEYWORDS

Sociality, oxytocin, dopamine, zebrafish, development, organizational hypothesis, social decision making network

Summary

Hormones regulate behavior either through activational effects that facilitate the acute expression of specific behaviors or through organizational effects that shape the development of the nervous system thereby altering adult behavior [1,2]. The neurohormone oxytocin (OXT) has an activational role in several aspects of social behavior [3], including social processing [4,5], attention [6,7] and reward [8], in rodents and humans. Previously, we showed that this activational role of OXT is evolutionarily conserved in deep time, since OXT also modulates perception of visual social cues [9] and social recognition [10,11] in zebrafish. In contrast, the organizational action of OXT neurons in maturation of distinct neural systems necessary for social behavior remains less explored. Here, we show that in zebrafish, OXT is required during early life for the display of social affiliation in adulthood. Perturbation of OXT neurons during early development led to a loss of dopaminergic neurons, associated with visual processing and reward, and altered the neuronal response to social stimuli in the preoptic area and the ventral telencephalon of the adult brain. Ultimately, adult fish which were ablated in early life, displayed altered functional connectivity within social decision-making brain nuclei both in naïve state and in response to social stimulus and became less social. We propose that OXT neurons have an organizational role, namely to shape forebrain neuroarchitecture during development and to acquire an affiliative response towards conspecifics.

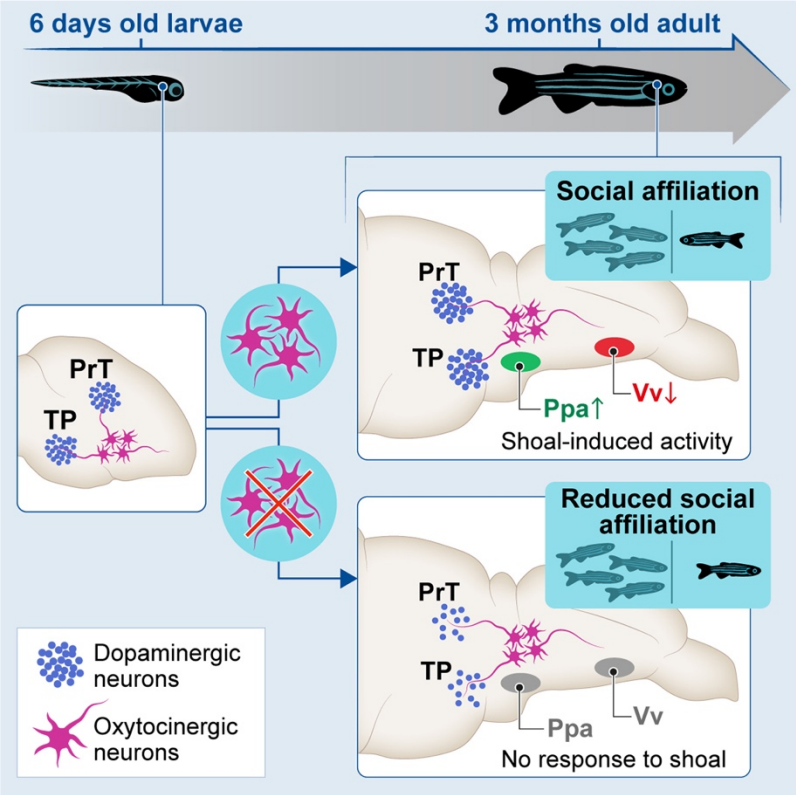

In brief:
Social behavior is developed over the lifetime of an organism, beginning at early developmental stages. We show that proper behavioral and neural response to social stimuli depend on a developmental process orchestrated by oxytocin neurons that are also necessary for development of dopaminergic neurons in visual processing (PrT) and reward (TP) centers.

Highlights:

- Ablation of oxytocinergic neurons during early development reduces social affiliation
- Ablated oxytocinergic neurons recover but their developmental perturbation leads to irreversible reduction in dopaminergic cell number.
- Early-life perturbation of oxytocinergic neurons blunts neuronal response to social stimulus in adulthood
- Modular structure of functional connectivity of social decision-making network changes as a result of early life OXT ablation

RESULTS

Early life ablation of oxytocinergic neurons decreases social affiliation

Zebrafish is a highly gregarious species exhibiting well-characterized social behaviors (reviewed in [12]). We quantified the visually-mediated motivation of zebrafish to approach conspecifics, as an indicator of social affiliation, by performing a two-choice preference test measuring the time that individuals spend either near a compartment containing a shoal of conspecifics or an empty one [10,11]. When an adult zebrafish is visually presented with both shoal and non-shoal compartments, in a side-by-side configuration, it will spend most of the time in association with the shoal; however, if shoal is not visible, fish tend to explore the entire arena (Figure1 A,B). In accordance with previous reports [13,14], we found social affiliation is an acquired developmental trait that emerges after the third week of life. This was observed both in zebrafish that were repeatedly exposed to the social affiliation behavioral arena throughout development (12 days-old (d):p=0.34, n=16; 19d: p=0.48, n=18; 21d: p=0.85, n=6; 26d: p=0.76, n=10; 36d: p=0.0007, n=13; 90d: p<0.0001, n=24; one sample t-test vs. theoretical score of 0.5 indicating no preference, Figure 1C), and in zebrafish that were only exposed to the arena once at a specific developmental time point to avoid habituation to the setup (12d: p= 0.69, n=15; 14d: p=0.91, n=14; 16d: p=0.73, n=15; 16d: p=0.88, n=17; 22d: p=0.049, n=12; 24d: p=0.07, n=18; 26d: p=0.01, n=17; 28d: p=0.057, n=13; 30d: p=0.17, n=8; 33d: p<0.0001, n=14; 62d: p=0.002, n=10; one sample t-test vs. theoretical score of 0.5 indicating no preference, Figure 1C).

Oxytocin (OXT) has long been known to regulate social behaviors across species [15] and it has been linked to neurodevelopmental disorders that impact social behavior during development and adulthood [16,17]. This makes OXT a good candidate system for investigating neurodevelopmental processes linked to social development. To disentangle the organizational vs. activational effects of OXT neurons in the acquisition of adult social affiliation, we used a transgenic line, *Tg(oxt:Gal4;UAS:NTR-mCherry)*, to express nitroreductase (NTR) protein fused to the mCherry reporter, in oxytocin neurons (Figure1D,E). In the presence of the drug metronidazole (MTZ), NTR produces cytotoxic metabolites, thereby allowing temporally controlled ablation of OXT neurons at different

developmental stages [18,19]. We confirmed the expression of the NTR-mcherry fusion protein in the OXT-ergic neuronal population by co-localizing the *Tg(oxt:Gal4;UAS:NTR-mCherry)* with a transgenic reporter *Tg(oxt:EGFP)* at different stages of development (8, 14, 24 and 90 days-old, Figure 1E).

In both mammals and fish, OXT is produced by specific cells in the preoptic hypothalamus which can be classified as magnocellular or parvocellular, based on soma size [20,21]. We and others have previously shown that zebrafish magnocellular OXT cells are clustered in the anterior-dorsal portion of the cell group, whereas the parvocellular neurons make up the more ventral part of the group [22,23]. We observed that the NTR-mCherry protein was prominently expressed in the most anterior-dorsal part of the preoptic area (Figure 1E), thus it can be considered to localize mainly to magnocellular OXT neurons in both larvae and adult zebrafish. MTZ treatment at all time points was highly effective (>80% decrease) at ablating NTR-mCherry-positive OXT neurons (Figure S1A,B, related to Figure 2). To ensure proper ablation of endogenous OXT-ergic cells following MTZ treatment, we also performed fluorescent *in situ* hybridization with probes directed against *oxt* mRNA at 4-6 days-old, 12-14 days-old, and in the adult (Figure 2A-C). A significant decrease in OXT-expressing cells was observed following MTZ treatment at all tested ages ($p= 0.0024$ n=11/10, $p=0.0003$ n=7/7, $p=0.0079$ n=5/4, for 4-6 days-old, 12-14 days-old, and adult ablation untreated/treated, respectively, one tailed Mann-Whitney test, Figure 2A'-C') .

To assess the effects of temporal OXT neuronal ablation on adult social affiliation, zebrafish were treated with MTZ at specific time-points during development (4-6, 12-14, 22-24 days-old) or post-puberty (90 days-old) and social affiliation was assessed in adulthood in comparison to untreated siblings (Figure 2D). We analyzed the social affiliation scores of eight independent cohorts in which OXT neurons were ablated at 4-6 days days-old and found that despite considerable variation among cohorts during the test, there was a robust effect of MTZ treatment on adult social affiliation (cohorts: $p= 0.0081$; treatment: $p=0.001$, see Methods section for detailed statistics of the Generalized Linear Model (GLM) with beta regression, Table S1, Figure S2A). MTZ treatment did not affect overall fish locomotion as measured by the total distance traveled during the trial

(cohorts: p=8.342e-16, treatment: p=0.668, Linear Model (LM), Table S1, Figure S2B). We also observed variation among control adult cohorts not expressing NTR but treated or untreated with MTZ at 4-6 days-old, without a main effect of MTZ-treatment on either social affiliation score (cohort: p=0.0001, MTZ-treatment: p=0.2653, GLM with beta regression, Table S2, Figure S2C) or total distance moved (cohort: p<2e-16, MTZ-treatment: p=0.1536, LM, Table S2, Figure S2D).

In view of the biological variability observed across cohorts, we further verified the effect of early-life OXT-neuron ablation on social affiliation by utilizing a Monte Carlo (MC) simulation where we randomly sampled 15 treated and 15 untreated 4-6 days-old larvae from all 8 cohorts and repeated the procedure for 1000 iterations. This analysis also clearly indicated an impairment of adult social affiliation (p<0.0001, one-tailed Mann-Whitney test, Figure 2E, see Statistics for details on MC), which was maintained in 12-14 days-old MTZ-treated adult fish (p=0.034, n=14/14, one-tailed Mann-Whitney test, Figure 2E).

In contrast to the deficit in social affiliation caused by early life MTZ treatment, ablation of OXT neurons in either 22-24 days-old juveniles or 90+ days-old adults did not affect adult social affiliation (22-24: p=0.1364, n=10/9 one-tailed Mann-Whitney test; Adults: p=0.3566, n=6/7, one-tailed Mann-Whitney test, Figure2E). This result coincides with the observation that social affiliation is a developmentally acquired trait which is established before the juvenile stage of development (Figure 1C and [14]).

Taken together, these results show that early developmental, but not adult, ablation of OXT neurons leads to a long-term deficit in social affiliation in adulthood, suggesting that OXT neurons are involved in an early-life developmental process that is required for proper social affiliation later in life.

Early life OXT ablation leads to impairments in specific dopaminergic clusters

Notably, although early-life OXT neuronal ablation induced an impairment in social affiliation, we observed complete recovery of the OXT neural population by adulthood, as ablated fish displayed normal counts of OXT-expressing NTR-mCherry transgene (4-6

days-old MTZ-treated (n=14) vs. untreated (n=15) adult zebrafish: p= 0.33, unpaired t-test, Figure2F-H). This is in line with previous work showing that zebrafish neurons are capable of regenerating following lesions even in adulthood [24]. Conversely, animals in which OXT neurons were ablated in adulthood displayed normal social drive (Figure 2E) despite the fact that the ablated cell populations had not yet recovered by the time of the behavioral testing (Figure 2C, S1).

We therefore hypothesized that the developmental organization of other neuronal systems that regulate social affiliation might have been affected by early OXT ablation. Dopamine (DA) is mainly involved in reward and reinforcement systems [25,26], but also in sensory modulation and attention gating [25,27]. DA neurons are activated during social interactions and mating, and interact with the OXT system to promote pair-bond formation [26,28] and sociability [29], suggesting that OXT and dopamine are both necessary to promote the sensory and rewarding aspects of social interactions. Therefore, we examined whether early perturbation of the OXT neuronal system affected specific tyrosine hydroxylase (TH)- positive DA-ergic neuronal clusters, which in zebrafish are anatomically discernible from other TH-positive catecholaminergic cells [30,31], and whether these effects persist over the long term. We observed that already 24 hours after ablation of OXT neurons at 4-6 days-old, there was a significant decrease in dopaminergic neuronal counts in the pretectum (PrT; p=0.009, n=18/18, LM, Figure 3A, Table S3), and the large neurons of the posterior tuberculum (TP; p=0.0045, n=18/18, LM, Figure 3A, Table S3). In contrast, no differences were found in telencephalic DA neurons of the ventral subpallium area (Table S3). The pretectum is the teleostean homologue of the superior colliculus, an area known to be involved in gaze control and possibly attention in zebrafish [32] as well as in mammals [33]. The posterior tuberculum is the of source of the ascending DA system, which is considered analogous to the mammalian ventral tegmental area (VTA) [30], which is involved in reward and reinforcement [34].

Unlike the ablated OXT cells, which recovered over time, the deficits in DA neurons observed in early OXT-ablated larvae persisted through adulthood, as adult fish that had been treated with MTZ between 4-6 days-old displayed a reduced number of TH-positive

DA cells in the PrT (p=0.005, n=7/7; Figure 3B, GLMM). Similarly, OXT ablation caused a decrease in the DA-ergic neurons residing in two subdivisions of the TP, the periventricular nucleus of the posterior tuberculum (TPp) and the posterior tuberal nucleus (PTN), which are distinguishable only in the adult (TPp p= 0.025, n=7/7; PTN p= 0.005, n=7/7; Figure 3B, GLMM). (GLMMs with Poisson regression, planned comparisons and fdr corrections, Figure S3 and Table S3).

To demonstrate that at the time of their ablation, OXT neurons physically interact with the affected DA neurons, we examined whether OXT neurons form synapses on DA-ergic clusters of the PrT and TP. We employed a double transgenic line, *Tg(oxt:Gal4;UAS:Sypb-EGFP)*, which genetically expresses the synaptic marker, synaptophysin-GFP in OXT neurons [35], and visualized synaptic contacts onto TH positive DA-ergic neurons (Figure 3C,D). To ensure that these are indeed bona-fide OXT releasing synapses, we also co-stained these fish with an anti-OXT antibody [35,36] (Figure 3D-F). We found OXT projections forming multiple synapses onto the DA neurons of the PrT and the TP (Figure 3D-F). We also observed OXT cells directly abutting the TH-positive cells of the TP (Figure 3F), raising the possibility that OXT affects nearby DA-ergic cells in a non-synaptic manner as has been shown in other species [37,38]. These results indicate that these two systems, DA and OXT, are already linked at early developmental stages and that early ablation of OXT neurons irreversibly impairs the development of subsets of DA neurons which are key for social affiliation later in life.

Early-life ablation of oxytocinergic neurons leads to impaired social information processing

In view of these results, we next examined whether these long-lasting developmental changes also manifested in the neural processing response to social stimuli in adults, focusing on vertebrate social decision-making network and mesolimbic reward system [39]. To this end, early-life ablated (MTZ-treated at 4-6 days-old) adult zebrafish were exposed to a single visual social stimulus for 10 minutes (a shoal of conspecifics comprised of 2 females and 2 males or an empty tank for controls) and their forebrain neuronal activity state was analyzed by immunostaining of phosphorylated ribosomal

protein S6 (pS6), a known correlate for neuronal activation ([40], Figure 4A). We then quantified the number of pS6-positive neurons in several specific brain areas known to be implicated in neural processing of social information and social reward [39] (Figures 4B-E and S5). Results showed that early OXT ablation significantly affected neuronal activity in response to social stimulus in two specific areas: the anterior part of the parvocellular preoptic nucleus (Ppa) and in the most anterior part of the ventral nucleus of ventral telencephalon (Vv) (GLMM with Poisson regression, planned comparisons and false discovery rate (fdr) corrections, Table S5).

Specifically, we found that while unablated fish exhibited increased activity in the Ppa upon exposure to a shoal of conspecifics, this was not observed in early ablated fish (untreated shoal vs untreated empty, p= 0.024, n= 11/7 respectively; MTZ-treated shoal vs MTZ-treated empty, p=0.88, n=10/6 respectively; Figure 4B,C, Table S5). Conversely, Vv neurons of unablated fish exhibited decreased activity upon exposure to a social stimulus, whereas early ablated animals maintained their neuronal activity regardless of the stimulus (untreated shoal vs untreated empty, p= 0.024, n=11/7 respectively; MTZ-treated shoal vs MTZ-treated empty, p=0.88, n= 11/7 respectively; Figure4 D,E; Table S5).

These results show that these two brain areas display deficits in neuronal response to a social stimulus in early OXT-ablated zebrafish. Importantly, the Vv is considered analogous to the mammalian lateral septum (LS), while the Ppa is analogous to the mammalian preoptic hypothalamus (POA) [39,41]. These areas are core nodes of the social behavior network in all vertebrate species and have a strong reciprocal connection with each other [39,41].

We next examined whether early-life ablation of OXT neurons in the POA altered functional connectivity between forebrain nuclei belonging to the social decision-making network (SDMN; [42]), by comparing the correlation matrices of activity levels for the different areas between ablated and non-ablated fish in either basal state or in response to social stimulus. We constructed correlation matrices corresponding to each treatment via a resampling scheme, inspired by Quadratic Assignment Procedure [43], that

additionally allows to choose the threshold for sparsification on the basis of minimal heterogeneity across resampled correlation matrices (see Methods). To identify functional reconfigurations between different treatments, we identified mesoscale differences in the way the functional networks are organized by their modular (or community) structure. To extract such modules, we performed community detection using the Leiden algorithm [44] on the functional connectivity matrix of each treatment. To ensure the robustness of the resulting partitions, we repeated the optimization 400 times per treatment and reconciled the different candidate partitions by considering the central partition [45] (see final partitions in Figure 4F). Already by visual inspection it is possible to observe differences in the overall community structure between treatments in the allocation of nodes to communities, and in the relative integration within and across communities. We quantified such integration by calculating the ratio r of the total edge weights within communities to the total edge weights between different communities (see Methods). We found that in the basal state (i.e. when no visual stimulus was presented) the mesoscale functional organization is different between ablated $(r = 4.6)$ and non-ablated fish $(r = 7.5)$, implying that the ablation of OXT neurons in the POA modifies the resting state networks of the forebrain SDMN. In particular, ablated fish show a much less segregated network with respect to non-ablated ones. Secondly, we observed that, in response to the social stimulus (i.e. sight of a conspecific shoal), the functional network of non-ablated fish transitions from a segregated state $(r = 7.5)$ to a more integrated one $(r = 3.7)$, whereas ablated fish showed the opposite pattern, moving from a more integrated basal state $(r = 4.6)$ to a more segregated response network $(r = 6.4)$. All r values are significantly different from zero, and also significantly different from each other $(p < 0.01)$. Finally, we completed the network analysis focusing on local differences in terms of network centralities. In particular, we looked at the strength of nodes, representing how strongly a node is connected to its neighbors (Table S.6). We found a strong and significant anti-correlation between the ranking of strengths for the ablated versus non-ablated fish in response to the social stimulus (Untreated Shoal vs MTZ-treated Shoal, Spearman r=-0.5, p=0.01), implying that the hub nodes for non-ablated fish are poorly connected nodes for the ablated and vice versa. Specifically, in untreated fish exposed to the social stimulus, the most connected nodes were the posterio-ventral part

of the ventral telencephalon (Vv_p), followed by the medial zone of the dorsal telencephalic area (Dm), two regions that have been implicated in the regulation of social interactions and motivated behavior in zebrafish [46,47]. In contrast, both these nodes drop their centrality in the SDMN network of MTZ-treated fish exposed to the social stimulus (from 1st to 5th and from 2nd to 16th, among 16 nodes, respectively), where the anterio- dorsal part of the ventral telencephalon (Vd_a) and the lateral part of the ventral telencephalon (Vl), two poorly connected nodes in untreated fish (ranking 14th and 16th, out of 16 nodes, respectively), were the most connected nodes (Table S6).

These results indicate that early-life OXT ablation leads to blunted response to shoal-induced changes in brain activity within specific nuclei (Vv and Ppa), and to a wide-ranging alteration in network connectivity spanning several nuclei of the social decision-making network in both basal state and in response to social stimulus.

Taken together, our results show that proper response to social stimuli depends on orchestrated co-development of OXT and DA neurons. We show that during development, OXT has important organizational effects. Early developmental perturbation of OXT neurons led to reduced attraction towards conspecifics, impaired the neurodevelopment of specific DA-ergic neurons, caused a blunted neural response to social stimuli in the forebrain (Ppa and Vv), and altered the connectivity of the SDMN.

DISCUSSION

Previous research has implicated OXT in various developmental disorders that affect social function in humans, have highlighted its importance in social behavior in animals, and indicated the importance of its communication with other systems, such as DA, serotonin and estrogen for proper social behavior [5,16,27,48,49]. However, there has been limited investigation into the mechanistic aspects of OXTs developmental functions, and how they are linked to its well-described social roles.

Here we utilize temporally controlled perturbations of OXT-ergic cells at different developmental timepoints during zebrafish life to show that OXT has a distinct developmental function, namely to enable proper development of specific downstream

DA-ergic clusters known to be involved in visual attention gating and reward [32,39]. We also show that in animals where this developmental process was perturbed, the response to social stimuli is affected, and social motivation is reduced.

The developmentally affected DA-ergic clusters, namely the pretectum/superior colliculus and the TPp/VTA have been linked in other organisms to social functioning at the level of behavior and, at the molecular level, to the OXT system. Thus, in primates and humans, which like zebrafish are highly dependent on vision for gathering social information, OXT receptors are expressed in the superior colliculus [50–53], and OXT modulates the gaze and oculomotor responses controlled by this nucleus [54,55]. This is also true of the VTA, where OXT receptors are expressed, which functions to promote sociability [29]. Notably, rhesus monkeys subjected to early social deprivation displayed a reduction in DA neurons of the VTA [56], and mouse KO of the autism-associated gene Nlgn3 resulted in impaired OXT signaling in DA-ergic neurons and aberrant activity in the DA-ergic neurons of the VTA [57]. This further shows how early perturbations to the OXT system can lead to wide-ranging and varied effects on other socially relevant systems in the brain. Whether the changes in DA-ergic neurons, caused the observed changes in social affiliation and neural activity has yet to be directly tested.

Specifically, we show that in normal fish, neurons of the Ppa respond to social stimuli by increased activity, while neurons of the Vv respond by reducing their activity. In contrast, in developmentally perturbed animals these areas do not change their activity following presentation of the stimulus. Importantly, the Vv is considered analogous to the mammalian lateral septum (LS), and the Ppa is analogous to the mammalian preoptic hypothalamus (POA) [39,41]. In zebrafish, the Vv/LS has been functionally associated with social affiliation, mainly through its cholinergic neurons [46]. However, it is interesting to note that in many animal models (e.g. rodents, teleosts, and cartilaginous fish), including zebrafish, the Vv/LS has been shown to contain mainly GABAergic neurons, and to be a source of GABAergic input to the VTA, a putative homologue of the TP, encompassing the TPp and PTN, in zebrafish [39], as well as the POA [39,58]. Thus, it is possible that the observed reduced activity in Vv/LS corresponds to GABAergic neurons that project to the Ppa and TP. These areas are core nodes of the social behavior network

in all vertebrate species and have a strong reciprocal connection with each other [39,41]. This suggests that social stimuli could promote a disinhibition in these target areas, which would be associated with the rewarding and/or motivational component of social affiliation. As a corollary, in early-ablated animals, where Vv activity remains high in response to social stimuli, the TP would remain inhibited, and the rewarding component of social affiliation would be attenuated, leading to decreased display of this behavior.

In addition, we show that the overall coactivation patterns of forebrain nuclei involved in social processing are altered in developmentally perturbed animals, both at baseline and following presentation of a social stimulus. In other words, we show that the connectivity between the different nodes of the social decision-making network changes as a result of early life OXT ablation. We submit that the proper maturation of this network at the level of neural architecture is dependent on early-life signaling by OXT neurons.

In summary, our results demonstrate that OXT neurons are required for the developmental acquisition of social affiliation and exert an organizational effect on other neuronal populations. Furthermore, our results suggest that this role involves orchestrating the co-development and maturation of several brain systems, such as the midbrain social visual processing and attention systems (the pretectum), social decision-making areas in the forebrain and ascending dopamine centers associated with reward. When the OXT-dependent developmental process is perturbed, neural responses to social stimuli in these regions become compromised, important parts of the social decision-making network fail to synchronize their activity, and eventually, the propensity to spend time near a shoal of conspecifics is reduced.

ACKNOWLEDGMENTS

We thank all members of Gil Levkowitz´s and Rui Oliveira´s laboratories for fruitful discussions, Nitzan Konstantin for English editing and Genia Brodsky for graphical abstract illustration. We thank the technical support of IGC's Advanced Imaging Facility (AIF-UIC), which is supported by the national Portuguese funding ref# PPBI-POCI-01-0145-FEDER-022122, co-financed by Lisboa Regional Operational Programme (Lisboa

2020), under the Portugal 2020 Partnership Agreement, through the European Regional Development Fund (FEDER) and Fundação para a Ciência e Tecnologia (FCT, Portugal); all the staff from the Fish Facility platforms of Instituto Gulbenkian de Ciência, Portugal, and Weizmann Institute of Science, Israel, for animal care and valuable advice; Congento, which is supported by the funding ref# LISBOA-01-0145-FEDER-022170, co-financed by Lisboa Regional Operational Programme (Lisboa 2020), under the Portugal 2020 Partnership Agreement, through the European Regional Development Fund (FEDER) and Fundação para a Ciência e a Tecnologia (FCT; Portugal); IGC´s Histopathology Facility for technical support, help and valuable advices; the Advanced BioImaging and BioOptics Experimental Platform (ABBE Platform) of the Champalimaud Center for the Unknown (CCU) for all the technical support and help.

Funding: ARN was supported by a Short-Term EMBO fellowship (ASTF 420-2013), by the Weizmann´s Dean of Faculty postdoctoral fellowship at the Weizmann Institute, Israel, and by Fundação para a Ciência e Tecnologia (FCT; SFRH/BPD/93317/2013) at Instituto Gulbenkian de Ciência, Portugal. M.G., E.W. and J.B. were supported by Israel Science Foundation (#1511/16); United States-Israel Binational Science Foundation (#2017325); Sagol Institute for Longevity and Estate of Emile Mimran . G.L. is an incumbent of the Elias Sourasky Professorial Chair. This work was funded by the project LISBOA-01-0145-FEDER-030627 co-funded by the Programa Operational Regional de Lisboa (Lisboa 2020), through Portugal 2020 and the European Regional Development Fund (FEDER), and by the FCT/MCTES through national funds (PIDDAC).

Authors contributions:

ARN- Designed the research, performed experiments, analyzed data, wrote/revised manuscript; MG - Designed the research, performed experiments, analyzed data, wrote/revised manuscript; EW- Performed experiments; JB- Performed experiments; GP and MT- Performed network analysis; SAMV- Performed statistical analysis; GL- Designed the research, supervision, edited/revised manuscript; RO- Designed the research, supervision, edited/revised manuscript.

References

1. Phoenix, C.H., Goy, R.W., Geral, A.A., and Young, W.C. (1959). Organizing action of prenatally administered testosterone propionate on the tissues mediating mating behavior in the female guinea pig. Endocrinology *65*, 369–82.
2. Adkins-Regan, E. (2012). Hormonal organization and activation: Evolutionary implications and questions. Gen. Comp. Endocrinol. *176*, 279–285.
3. Donaldson, Z.R., and Young, L.J. (2008). Oxytocin, vasopressin, and the neurogenetics of sociality. Science. *322*, 900–904.
4. Gamer, M., Zurowski, B., and Büchel, C. (2010). Different amygdala subregions mediate valence-related and attentional effects of oxytocin in humans. Proc. Natl. Acad. Sci. U. S. A. *107*, 9400–5.
5. Grinevich, V., and Stoop, R. (2018). Interplay between Oxytocin and Sensory Systems in the Orchestration of Socio-Emotional Behaviors. Neuron *99*, 887–904.
6. Bartz, J.A., Zaki, J., Bolger, N., and Ochsner, K.N. (2011). Social effects of oxytocin in humans: context and person matter. Trends in Cognitive Sciences, *15*, 301-309.
7. Shamay-Tsoory, S.G., and Abu-Akel, A. (2016). The Social Salience Hypothesis of Oxytocin. Biol. Psychiatry *79*, 194–202.
8. Insel, T.R., and Shapiro, L.E. (1992). Oxytocin receptor distribution reflects social organization in monogamous and polygamous voles. Proc. Natl. Acad. Sci. U. S. A. *89*, 5981–5.
9. Nunes, A.R., Carreira, L., Anbalagan, S., Blechman, J., Levkowitz, G., and Oliveira, R.F. (2020). Perceptual mechanisms of social affiliation in zebrafish. Sci. Rep. *10*, 1–14.
10. Ribeiro, D., Nunes, A.R., Gliksberg, M., Anbalagan, S., Levkowitz, G., and Oliveira, R.F. (2020). Oxytocin receptor signalling modulates novelty recognition but not social preference in zebrafish. J. Neuroendocrinol. *32*, e12834.
11. Ribeiro, D., Nunes, A.R., Teles, M., Anbalagan, S., Blechman, J., Levkowitz, G., and Oliveira, R.F. (2020). Genetic variation in the social environment affects behavioral phenotypes of oxytocin receptor mutants in zebrafish. Elife *9*.
12. Nunes, A.R., Ruhl, N., Winberg, S., and Oliveira, R.F. (2017). Social phenotypes

in zebrafish. In The Rights and Wrongs of Zebrafish: Behavioral Phenotyping of Zebrafish (Springer International Publishing), pp. 95–130.

13. Engeszer, R.E., Barbiano, L.A. DA, Ryan, M.J., and Parichy, D.M. (2007). Timing and plasticity of shoaling behaviour in the zebrafish, Danio rerio. Anim. Behav. *74*, 1269–1275.

14. Dreosti, E., Lopes, G., Kampff, A.R., and Wilson, S.W. (2015). Development of social behavior in young zebrafish. Front. Neural Circuits *9*, 1–9.

15. Goodson, J.L. (2008). Nonapeptides and the evolutionary patterning of sociality. Prog. Brain Res. *170*, 3–15.

16. Hovey, D., Zettergren, A., Jonsson, L., Melke, J., Anckarsäter, H., Lichtenstein, P., and Westberg, L. (2014). Associations between oxytocin-related genes and autistic-like traits. Soc. Neurosci. *9*, 378–386.

17. Pobbe, R.L.H., Pearson, B.L., Defensor, E.B., Bolivar, V.J., Young, W.S., Lee, H.-J., Blanchard, D.C., Blanchard, R.J., and Blanchard, R.J. (2012). Oxytocin receptor knockout mice display deficits in the expression of autism-related behaviors. Horm. Behav. *61*, 436–44.

18. Curado, S., Anderson, R.M., Jungblut, B., Mumm, J., Schroeter, E., and Stainier, D.Y.R. (2007). Conditional targeted cell ablation in zebrafish: a new tool for regeneration studies. Dev. Dyn. *236*, 1025–1035.

19. Curado, S., Stainier, D.Y.R., and Anderson, R.M. (2008). Nitroreductase-mediated cell/tissue ablation in zebrafish: a spatially and temporally controlled ablation method with applications in developmental and regeneration studies. Nat. Protoc. *3*, 948–954.

20. Sawchenko, P.E., and Swanson, L.W. (1982). Immunohistochemical identification of neurons in the paraventricular nucleus of the hypothalamus that project to the medulla or to the spinal cord in the rat. J. Comp. Neurol. *205*, 260–272.

21. Van den Dungen, H.M., Buijs, R.M., Pool, C.W., and Terlou, M. (1982). The distribution of vasotocin and isotocin in the brain of the rainbow trout. J. Comp. Neurol. *212*, 146–157.

22. Wircer, E., Blechman, J., Borodovsky, N., Tsoory, M., Nunes, A.R., Oliveira, R.F., and Levkowitz, G. (2017). Homeodomain protein otp affects developmental

neuropeptide switching in oxytocin neurons associated with a long-term effect on social behavior. Elife *6:* e22170.

23. Wee, C.L., Nikitchenko, M., Wang, W.C., Luks-Morgan, S.J., Song, E., Gagnon, J.A., Randlett, O., Bianco, I.H., Lacoste, A.M.B., Glushenkova, E., *et al.* (2019). Zebrafish oxytocin neurons drive nocifensive behavior via brainstem premotor targets. Nat. Neurosci. *22*, 1477–1492.
24. Kizil, C., Kaslin, J., Kroehne, V., and Brand, M. (2012). Adult neurogenesis and brain regeneration in zebrafish. Dev. Neurobiol. *72*, 429–61.
25. Love, T.M. (2014). Oxytocin, motivation and the role of dopamine. Pharmacol. Biochem. Behav. *119*, 49–60.
26. Dölen, G., and Malenka, R.C. (2014). The Emerging Role of Nucleus Accumbens Oxytocin in Social Cognition. Biol. Psychiatry *76*, 354–355.
27. Grinevich, V., Sophie Knobloch-Bollmann, H., Eliava, M., Busnelli, M., and Chini, B. (2015). Assembling the Puzzle: Pathways of Oxytocin Signaling in the Brain. Biol. Psychiatry.
28. Johnson, Z. V., Walum, H., Xiao, Y., Riefkohl, P.C., and Young, L.J. (2017). Oxytocin receptors modulate a social salience neural network in male prairie voles. Horm. Behav. *87*, 16–24.
29. Hung, L.W., Neuner, S., Polepalli, J.S., Beier, K.T., Wright, M., Walsh, J.J., Lewis, E.M., Luo, L., Deisseroth, K., Dölen, G., *et al.* (2017). Gating of social reward by oxytocin in the ventral tegmental area. Science. *357*, 1406–1411.
30. Rink, E., and Wullimann, M.F. (2001). The teleostean (zebrafish) dopaminergic system ascending to the subpallium (striatum) is located in the basal diencephalon (posterior tuberculum). Brain Res. *889*, 316–330.
31. Rink, E., and Wullimann, M.F. (2002). Connections of the ventral telencephalon and tyrosine hydroxylase distribution in the zebrafish brain (Danio rerio) lead to identification of an ascending dopaminergic system in a teleost. In Brain Research Bulletin, pp. 385–387.
32. Antinucci, P., Folgueira, M., and Bianco, I.H. (2019). Pretectal neurons control hunting behaviour. Elife *8* e48114
33. Krauzlis, R.J., Liston, D., and Carello, C.D. (2004). Target selection and the

superior colliculus: Goals, choices and hypotheses. In Vision Research, pp. 1445–1451.

34. Morales, M., and Margolis, E.B. (2017). Ventral tegmental area: Cellular heterogeneity, connectivity and behaviour. Nat. Rev. Neurosci. *18*, 73–85.

35. Anbalagan, S., Blechman, J., Gliksberg, M., Gordon, L., Rotkopf, R., Dadosh, T., Shimoni, E., and Levkowitz, G. (2019). Robo2 regulates synaptic oxytocin content by affecting actin dynamics. Elife *8*: e45650.

36. Blechman, J., Anbalagan, S., Matthews, G.G., and Levkowitz, G. (2018). Genome Editing Reveals Idiosyncrasy of CNGA2 Ion Channel-Directed Antibody Immunoreactivity Toward Oxytocin. Front. Cell Dev. Biol. *6*, 117.

37. Ludwig, M., and Leng, G. (2006). Dendritic peptide release and peptide-dependent behaviours. Nat. Rev. Neurosci. *7*, 126–36.

38. Son, S.J., Filosa, J.A., Potapenko, E.S., Biancardi, V.C., Zheng, H., Patel, K.P., Tobin, V.A., Ludwig, M., and Stern, J.E. (2013). Dendritic peptide release mediates interpopulation crosstalk between neurosecretory and preautonomic networks. Neuron *78*, 1036–49.

39. O'Connell, L.A., and Hofmann, H.A. (2011). The Vertebrate mesolimbic reward system and social behavior network: A comparative synthesis. J. Comp. Neurol. *519*, 3599–3639.

40. Knight, Z.A., Tan, K., Birsoy, K., Schmidt, S., Garrison, J.L., Wysocki, R.W., Emiliano, A., Ekstrand, M.I., and Friedman, J.M. (2012). Molecular profiling of activated neurons by phosphorylated ribosome capture. Cell *151*, 1126–1137.

41. Wullimann, M.F., and Mueller, T. (2004). Teleostean and mammalian forebrains contrasted: Evidence from genes to behavior. J. Comp. Neurol. *475*, 143–162.

42. O'Connell, L.A., and Hofmann, H.A. (2012). Evolution of a vertebrate social decision-making network. Science. *336*, 1154–1157.

43. Makagon, M.M., McCowan, B., and Mench, J.A. (2012). How can social network analysis contribute to social behavior research in applied ethology? Appl. Anim. Behav. Sci. *138*, 152–161.

44. Traag, V.A., Waltman, L., and van Eck, N.J. (2019). From Louvain to Leiden: guaranteeing well-connected communities. Sci. Rep. *9*, 1–12.

45. Peixoto, T.P. (2020). Revealing consensus and dissensus between network partitions. Available at: https://arxiv.org/abs/2005.13977v2.

46. Stednitz, S.J., McDermott, E.M., Ncube, D., Tallafuss, A., Eisen, J.S., and Washbourne, P. (2018). Forebrain Control of Behaviorally Driven Social Orienting in Zebrafish. Curr. Biol. *28*, 2445-2451.e3.

47. von Trotha, J.W., Vernier, P., and Bally-Cuif, L. (2014). Emotions and motivated behavior converge on an amygdala-like structure in the zebrafish. Eur. J. Neurosci. *40*, 3302–3315.

48. Heinrichs, M., von Dawans, B., and Domes, G. (2009). Oxytocin, vasopressin, and human social behavior. Front. Neuroendocrinol. *30,* 548-557

49. Rajamani, K.T., Wagner, S., Grinevich, V., and Harony-Nicolas, H. (2018). Oxytocin as a Modulator of Synaptic Plasticity: Implications for Neurodevelopmental Disorders. Front. Synaptic Neurosci. *10*, 17.

50. Freeman, S.M., Inoue, K., Smith, A.L., Goodman, M.M., and Young, L.J. (2014). The neuroanatomical distribution of oxytocin receptor binding and mRNA in the male rhesus macaque (Macaca mulatta). Psychoneuroendocrinology *45*, 128–141.

51. Freeman, S.M., Palumbo, M.C., Lawrence, R.H., Smith, A.L., Goodman, M.M., and Bales, K.L. (2018). Effect of age and autism spectrum disorder on oxytocin receptor density in the human basal forebrain and midbrain. Transl. Psychiatry *8*, 257.

52. Freeman, S.M., Walum, H., Inoue, K., Smith, A.L., Goodman, M.M., Bales, K.L., and Young, L.J. (2014). Neuroanatomical distribution of oxytocin and vasopressin 1a receptors in the socially monogamous coppery titi monkey (Callicebus cupreus). Neuroscience *273*, 12–23.

53. Schorscher-Petcu, A., Dupré, A., and Tribollet, E. (2009). Distribution of vasopressin and oxytocin binding sites in the brain and upper spinal cord of the common marmoset. Neurosci. Lett. *461*, 217–222.

54. Leknes, S., Wessberg, J., Ellingsen, D.-M., Chelnokova, O., Olausson, H., and Laeng, B. (2013). Oxytocin enhances pupil dilation and sensitivity to 'hidden' emotional expressions. Soc. Cogn. Affect. Neurosci. *8*, 741–749.

55. Kret, M.E., and De Dreu, C.K.W. (2017). Pupil-mimicry conditions trust in partners: Moderation by oxytocin and group membership. Proc. R. Soc. B Biol. Sci. *284*.

56. Martin, L.J., Spicer, D.M., Lewis, M.H., Gluck, J.P., and Cork, L.C. (1991). Social deprivation of infant rhesus monkeys alters the chemoarchitecture of the brain: I. Subcortical regions. J. Neurosci. *11*, 3344–3358.

57. Hörnberg, H., Pérez-Garci, E., Schreiner, D., Hatstatt-Burklé, L., Magara, F., Baudouin, S., Matter, A., Nacro, K., Pecho-Vrieseling, E., and Scheiffele, P. (2020). Rescue of oxytocin response and social behaviour in a mouse model of autism. Nature *584*, 252–256.

58. Vega-Quiroga, I., Yarur, H.E., and Gysling, K. (2018). Lateral septum stimulation disinhibits dopaminergic neurons in the antero-ventral region of the ventral tegmental area: Role of GABA-A alpha 1 receptors. Neuropharmacology *128*, 76–85.

59. Parker, M.O., Brock, A.J., Walton, R.T., and Brennan, C.H. (2013). The role of zebrafish (Danio rerio) in dissecting the genetics and neural circuits of executive function. Front. Neural Circuits *7*, 63.

60. Panula, P., Chen, Y.C., Priyadarshini, M., Kudo, H., Semenova, S., Sundvik, M., and Sallinen, V. (2010). The comparative neuroanatomy and neurochemistry of zebrafish CNS systems of relevance to human neuropsychiatric diseases. Neurobiol. Dis. *40*, 46–57.

61. Anbalagan, S., Gordon, L., Blechman, J., Matsuoka, R.L., Rajamannar, P., Wircer, E., Biran, J., Reuveny, A., Leshkowitz, D., Stainier, D.Y.R., *et al.* (2018). Pituicyte Cues Regulate the Development of Permeable Neuro-Vascular Interfaces. Dev. Cell *47*, 711-726.e5.

62. Davison, J.M., Akitake, C.M., Goll, M.G., Rhee, J.M., Gosse, N., Baier, H., Halpern, M.E., Leach, S.D., and Parsons, M.J. (2007). Transactivation from Gal4-VP16 transgenic insertions for tissue-specific cell labeling and ablation in zebrafish. Dev. Biol. *304*, 811–824.

63. Blechman, J., Amir-Zilberstein, L., Gutnick, A., Ben-Dor, S., and Levkowitz, G. (2011). The metabolic regulator PGC-1α directly controls the expression of the

hypothalamic neuropeptide oxytocin. J. Neurosci. *31*, 14835–40.

64. Meyer, M.P., and Smith, S.J. (2006). Evidence from in vivo imaging that synaptogenesis guides the growth and branching of axonal arbors by two distinct mechanisms. J. Neurosci. *26*, 3604–3614.

65. Schindelin, J., Arganda-Carreras, I., Frise, E., Kaynig, V., Longair, M., Pietzsch, T., Preibisch, S., Rueden, C., Saalfeld, S., Schmid, B., *et al.* (2012). Fiji: An open-source platform for biological-image analysis. Nat. Methods *9*, 676–682.

66. Machluf, Y., and Levkowitz, G. (2011). Visualization of mRNA expression in the zebrafish embryo. Methods Mol. Biol. *714*, 83–102.

67. Lorenzi, E., Mayer, U., Rosa-Salva, O., and Vallortigara, G. (2017). Dynamic features of animate motion activate septal and preoptic areas in visually naïve chicks (Gallus gallus). Neuroscience *354*, 54–68.

68. Tay, T.L., Ronneberger, O., Ryu, S., Nitschke, R., and Driever, W. (2011). Comprehensive catecholaminergic projectome analysis reveals single-neuron integration of zebrafish ascending and descending dopaminergic systems. Nat. Commun. *2*, 171.

69. Sallinen, V., Torkko, V., Sundvik, M., Reenilä, I., Khrustalyov, D., Kaslin, J., and Panula, P. (2009). MPTP and MPP+ target specific aminergic cell populations in larval zebrafish. J. Neurochem. *108*, 719–731.

70. Wullimann, M.F., Rupp, B., and Reichert, H. (1996). Neuroanatomy of the Zebrafish Brain (Birkhäuser Basel). DOI https://doi.org/10.1007/978-3-0348-8979-7.

71. De Vico Fallani, F., Latora, V., and Chavez, M. (2017). A Topological Criterion for Filtering Information in Complex Brain Networks. PLOS Comput. Biol. *13*, e1005305.

72. R core Team (2013). R: A language and environment for statistical computing.

73. Bates, D., Mächler, M., Bolker, B.M., and Walker, S.C. (2015). Fitting linear mixed-effects models using lme4. J. Stat. Softw. *67*.

74. Henrik Singmann, Ben Bolker, Jake Westfall, F.A. and M.S.B.-S. (2020). afex: Analysis of Factorial Experiments. R package version 0.27-2.

75. Lenth, R. (2020). emmeans: Estimated Marginal Means, aka Least-Squares

559 Means. R package version 1.4.7.

560

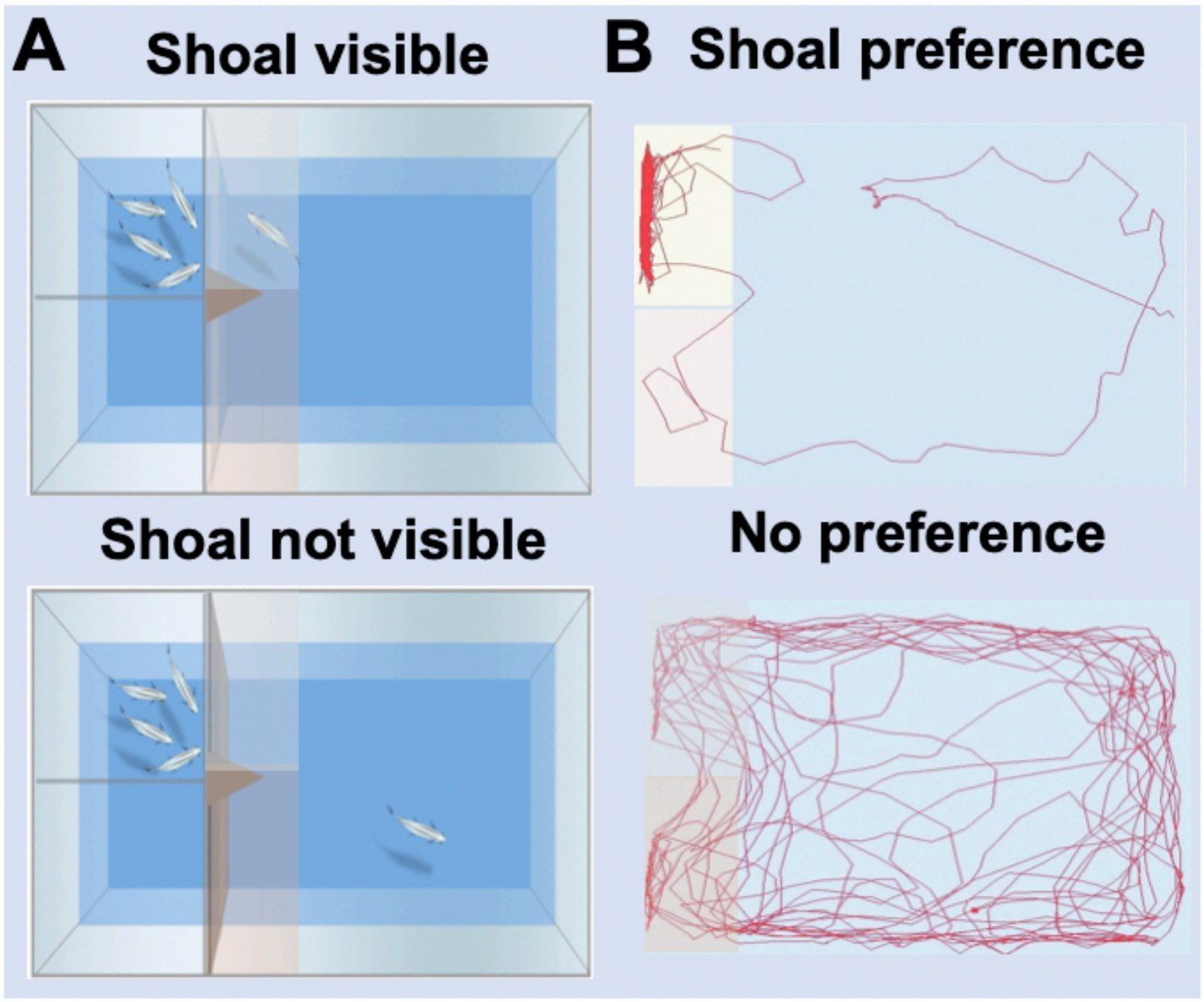

Fig.1

Figure 1. Behavioral and genetic tools to study the role of oxytocinergic neurons in adult social affiliation. (A,B) Schematic representation of the visual-mediated shoal preference behavioral test setup. (A) When a mixed-sex shoal stimulus is visible, focal fish spends most of the time near the shoal (top). When the shoal is not visible (bottom), the focal fish explores the entire arena equally. (B) Representative tracking of the focal fish behavior. (C) Ontogeny of social affiliation in zebrafish. Visual preference to associate with a shoal of conspecific fish (social affiliation score> 0.5) emerges after the third week of life. Social affiliation score = $\%T_{shoal}/(\%T_{shoal} + \%T_{non\text{-}shoal})$. # Hash indicates a significant preference towards conspecifics, determined by a one-sample *t*-test with a hypothesized value of 0.5 (chance level). Fish were tested either repeatedly throughout development (black squares, longitudinal group) or only once at certain developmental time points (grey squares, cross-sectional group). (D) Spatio-temporal control of oxytocin-specific transgene expression. *oxt*:Gal4 drives the expression of nitroreductase tagged with mCherry fluorescent protein (NTR-mCherry) in oxytocinergic neurons. (E) *Tg(oxt:Gal4;UAS-NTR-mCherry)* characterization: NTR-mCherry+ cells co-localized with a subpopulation of *oxt*:eGFP neurons, at all developmental stages studied (8, 14 and 24 days-old: whole-mount larvae confocal z-stack image, dorsal view, anterior to top; 90 days-old, close-up of the preoptic area (POA), sagittal brain slice, confocal z-stack image, anterior to left). Scale: 20 µm. (F) Percentage of co-localization of *oxt*:NTR-mCherry^{+} and *oxt*:eGFP^{+} neuronal population. Data presented as mean ± SEM.

**p<0.01, ~ p<0.1; # p<0.05, ## p<0.01, ### p<0.001, #### p<0.0001 (black # relates to the longitudinal group, grey # relates to the cross-sectional group).

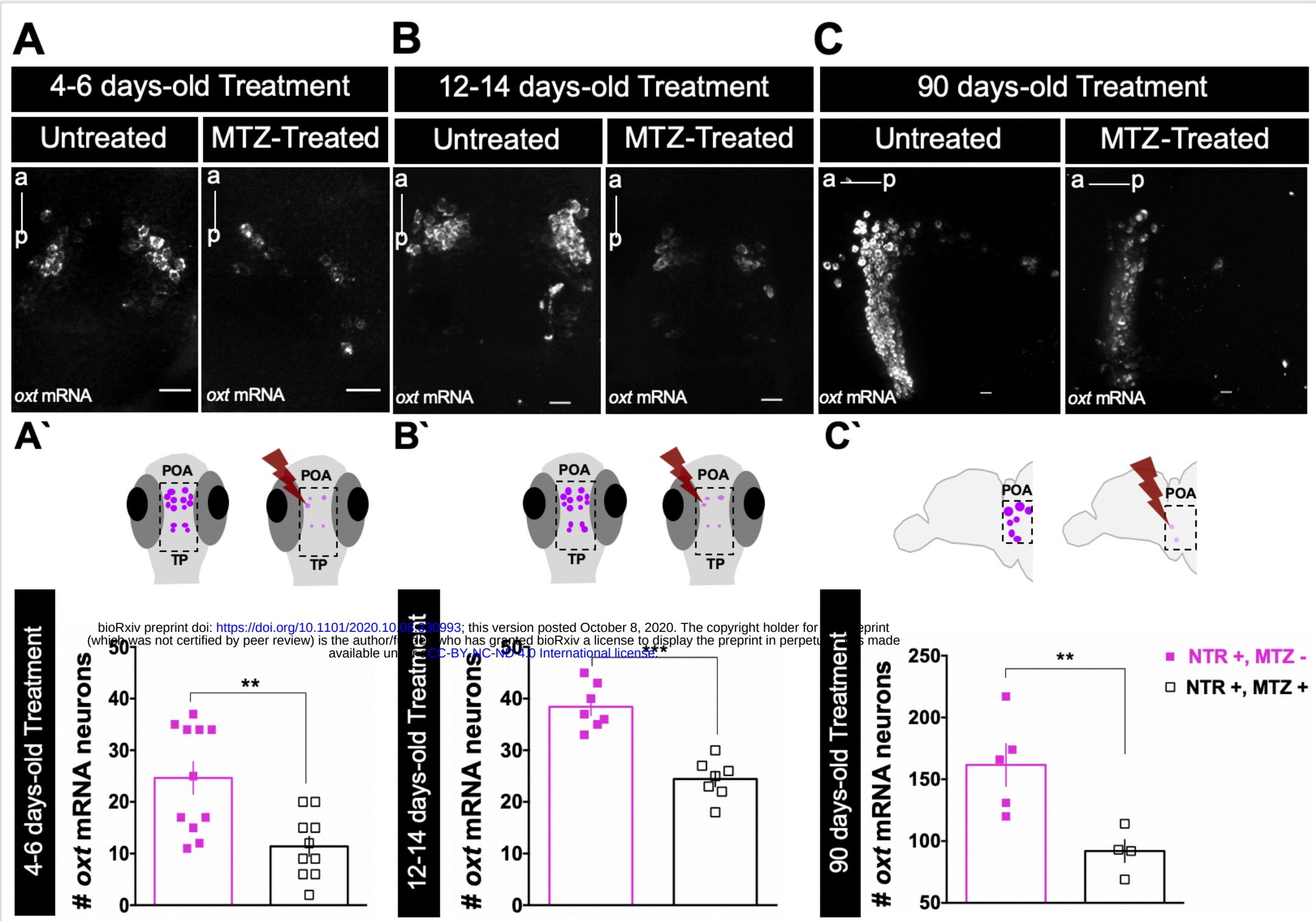

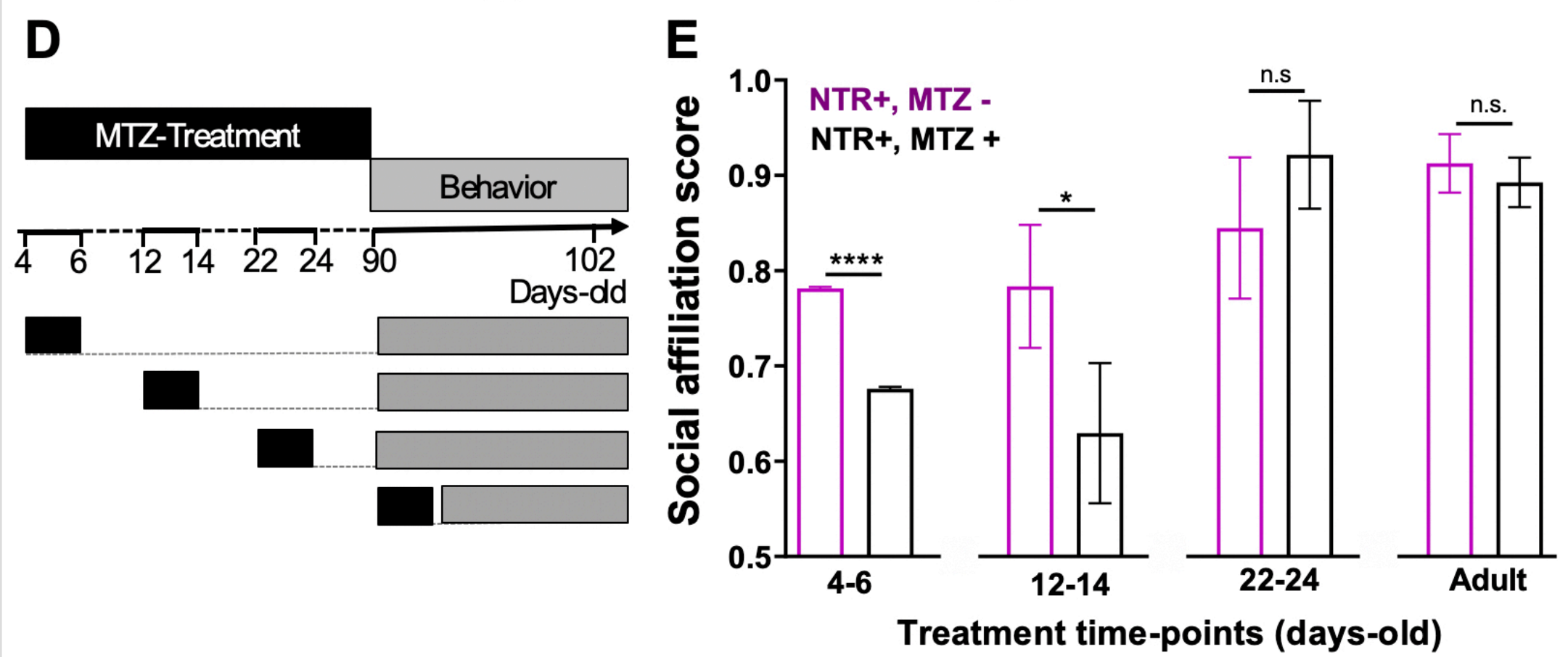

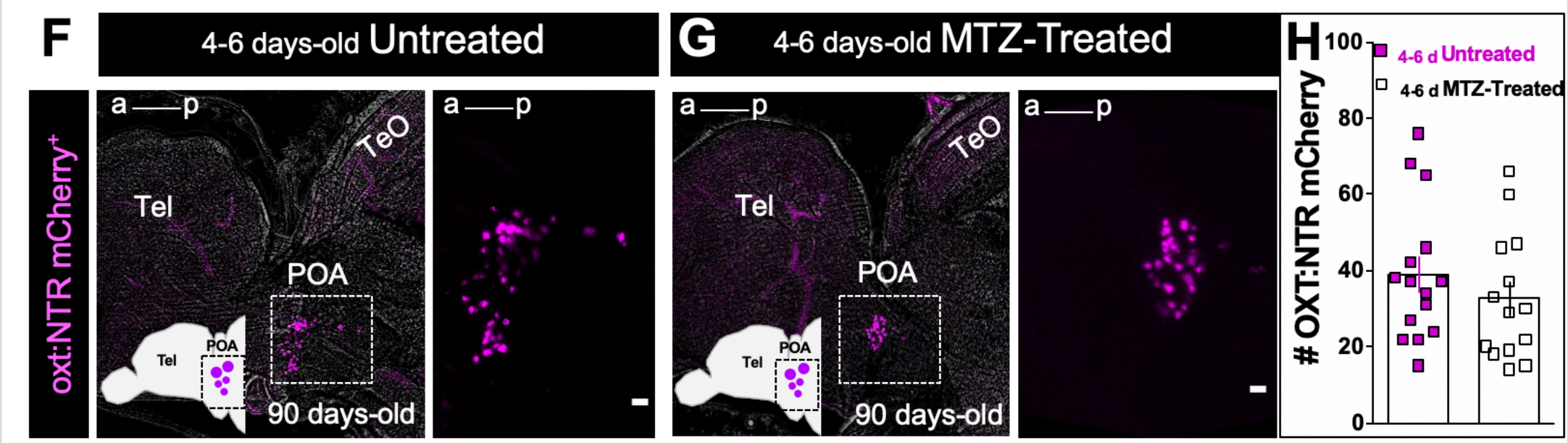

Fig.2

Figure 2. Contrasting organizational vs activational effects of oxytocin neurons in adult social affiliation. (A-C) Representative examples of the effects of metronidazole (MTZ)- induced ablation on endogenous OXT as detected by *in situ* hybridization, at different treatment time-points. (A) 4-6 days-old treatment and (B) 12-14 days-old treatment: whole-mount larvae confocal maximum intensity z-stack image, dorsal view, anterior to top; (C) 90 days-old treatment: sagittal brain slice, confocal maximum intensity z-stack image, anterior to left. Scale: 20 µm. (A´-C´) Quantification of the number of cells expressing OXT mRNA in untreated fish or following MTZ treatment at: (A´) 4-6 days-old treatment. (B´) 12-14 days-old treatment. (C´) 90 days-old treatment. (D) Experimental timeline: fish were MTZ-treated at different developmental stages, allowed to grow until adulthood and then tested for social affiliation. (E) MTZ treatments during the first two weeks of life, but not later, affect adult social affiliation. Social affiliation score = $\%T_{shoal}$ / ($\%T_{shoal}$ + $\%T_{non\text{-}shoal}$). Eight independent cohorts were treated at 4-6 days-old, and only one cohort at later time points. Therefore, in order to obtain comparable sample sizes among the different age-treatment groups and a more representative sample, the data for 4-6 days-old MTZ treatment shown in this graph were generated by a Monte Carlo simulation with 1000 iterations of samples of 15 individuals of each group (4-6 days-old MTZ-treated vs. untreated; see Statistical analysis subsection for details). Data presented as mean ± SEM. Full squares: untreated fish (NTR+, MTZ-); Open squares: MTZ-treated fish (NTR+, MTZ+), *p<0.05, **p<0.01,*** p<0.001. ****p<0.0001. One-tailed p-values were used because there was an *a priori* directional hypothesis that MTZ-treatment would ablate OXT neurons in fish expressing the NTR transgene and induce a decrease in social affiliation behavior. (F-H) OXT neurons ablated at 4-6 days-old were recovered by adulthood. (F) Representative example of NTR-mCherry-expressing OXT neurons in untreated adult fish. (G) Representative example of NTR-mCherry-expressing OXT neurons in adult fish treated with MTZ at 4-6 days-old. Images in (F,G) are maximum intensity confocal z-stacks, sagittal slices, anterior to left. (H) Quantification of the number of NTR-mCherry cells in untreated (full squares) and 4-6 days-old MTZ-treated adult fish (empty squares).

A

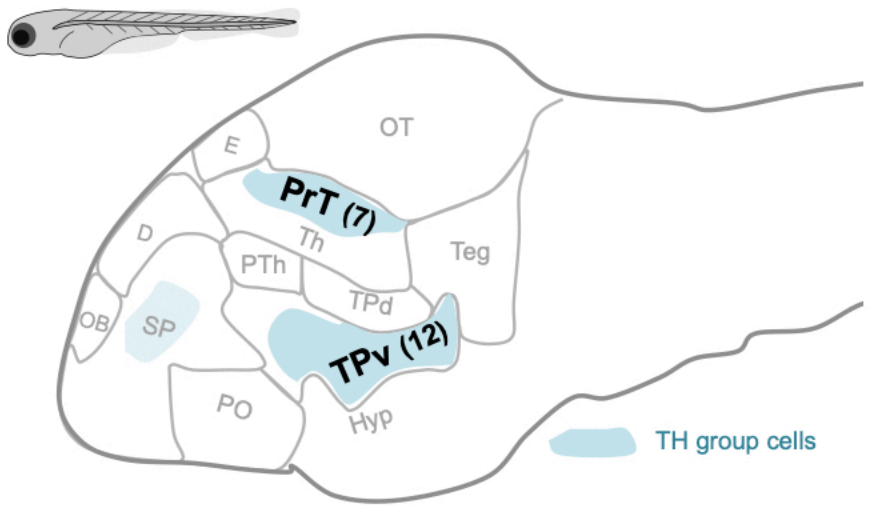

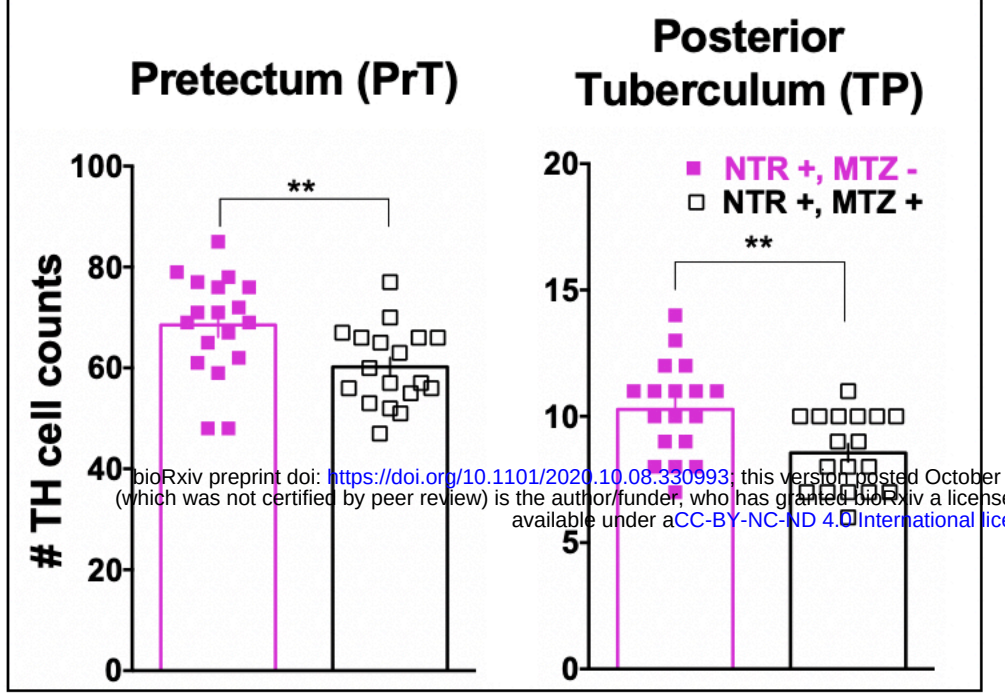

B

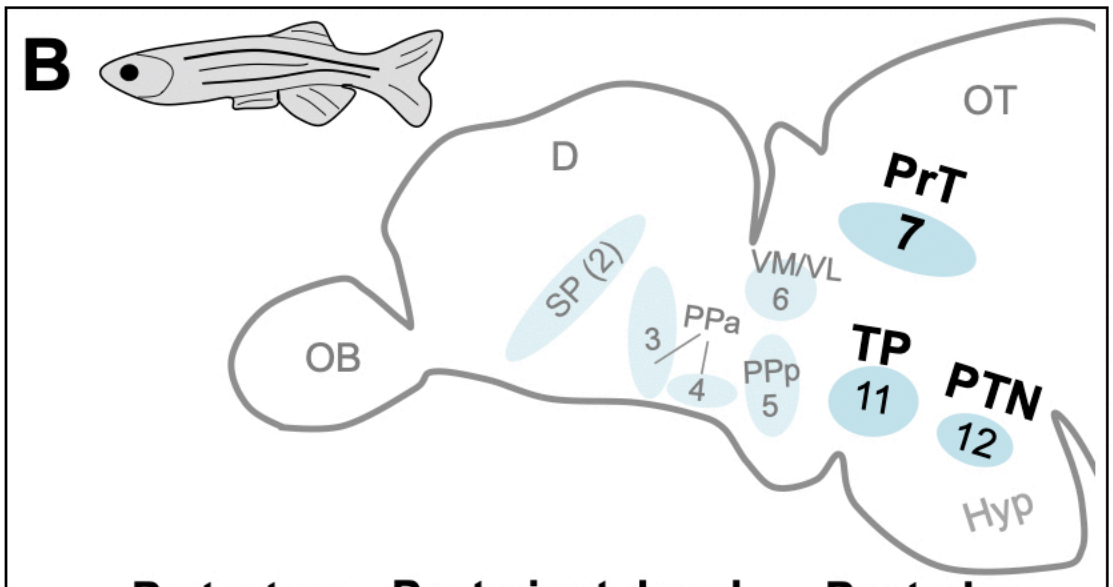

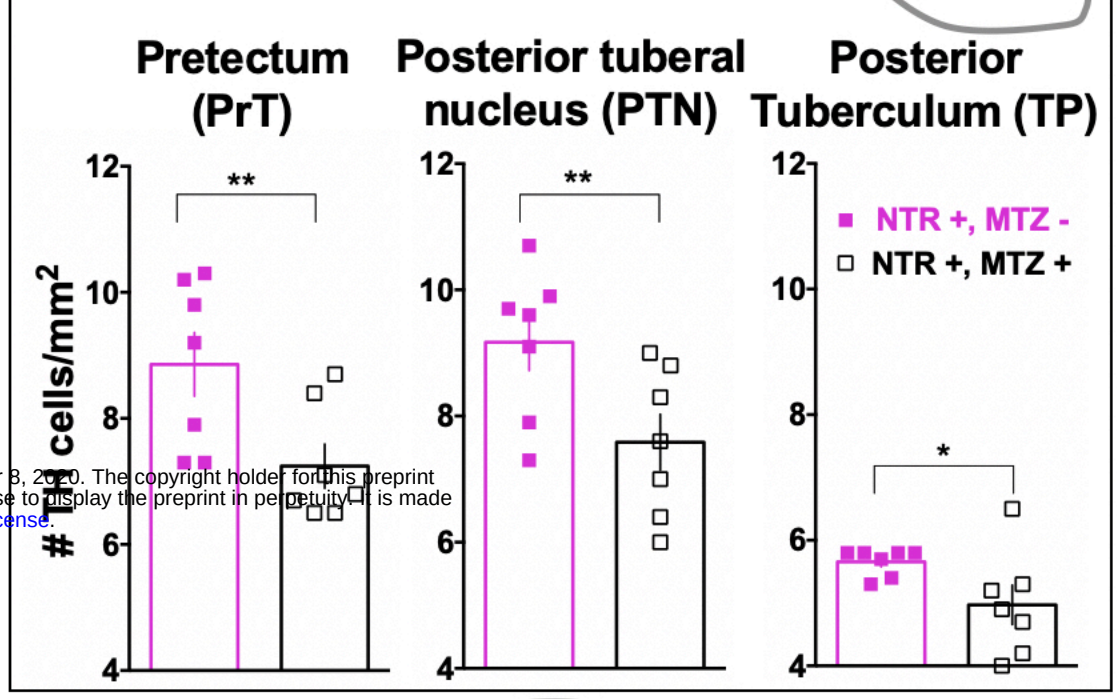

C

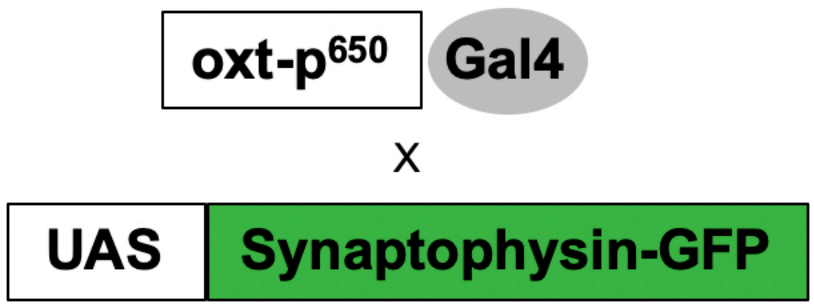

D

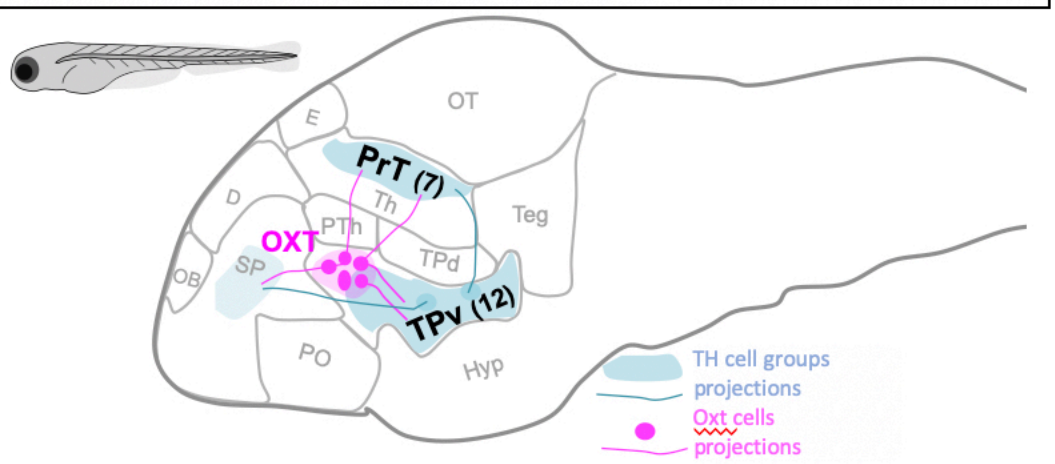

E

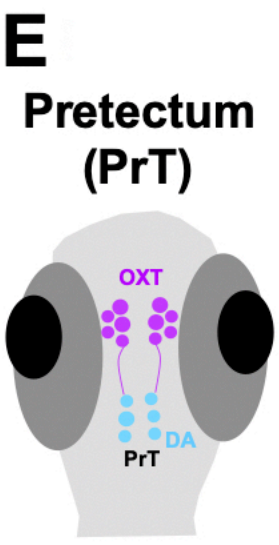

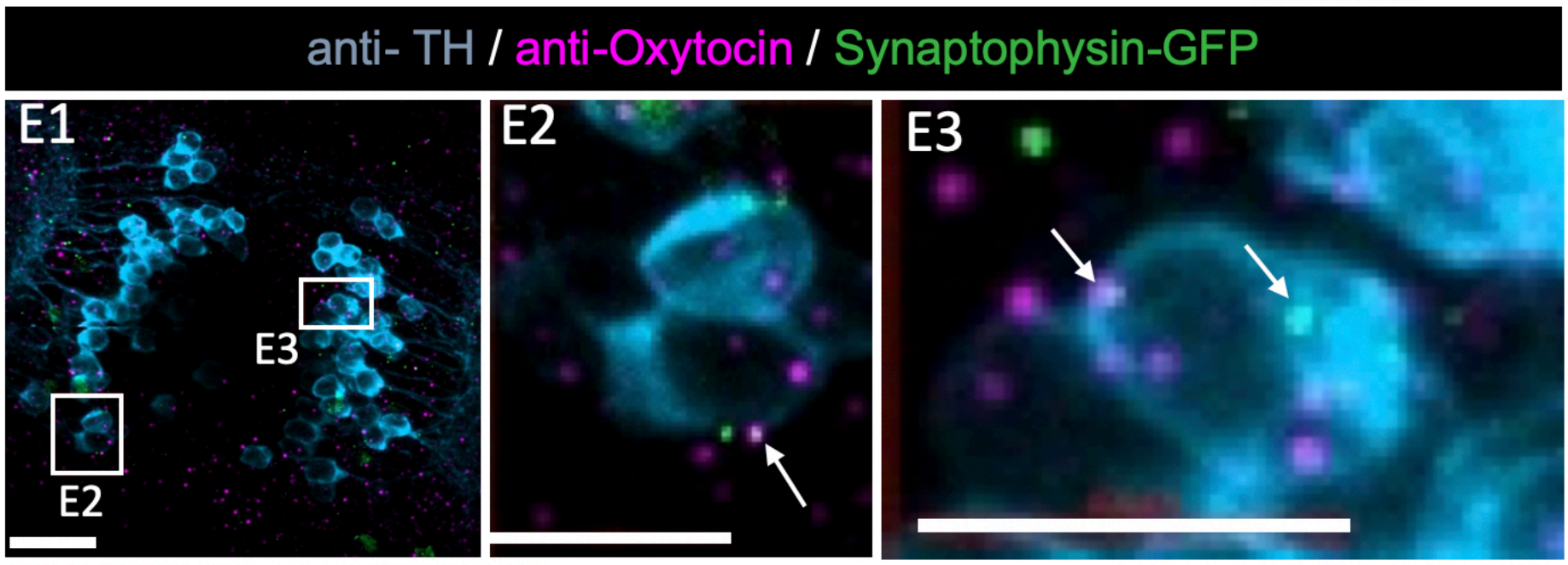

F

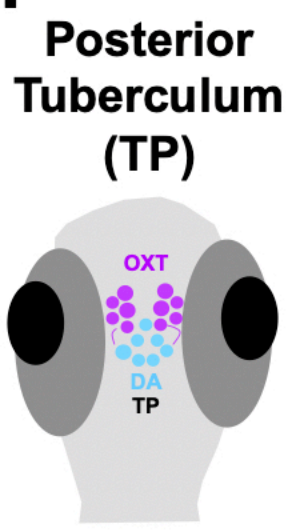

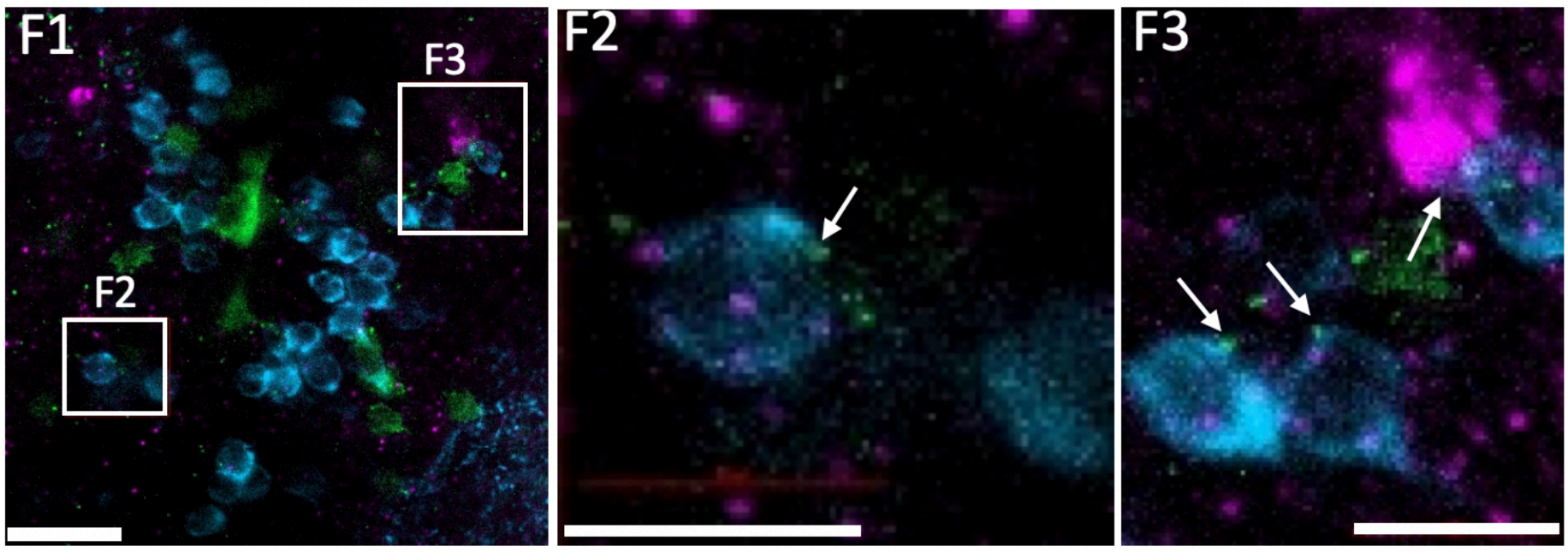

Fig.3

Figure 3. Early-life OXT ablation affects the dopaminergic system. (A) Top: Schematic sagittal section through a zebrafish larva brain showing the three dopaminergic clusters that were analyzed in this study, and highlighting two key dopaminergic brain areas that were affected by OXT neuronal ablation at 4-6 days-old, namely the pretectum (PrT) and posterior tuberculum (PT). Schematic was adapted from *zebrafishucl.org/forebrain-regions/posterior-tuberculum*. Bottom: Quantification of total TH cell counts in untreated (NTR+, MTZ-) vs 4-6 days-old MTZ-treated (NTR+, MTZ+) larvae. (B) Top: Schematic sagittal section through a zebrafish adult brain, showing the eight dopaminergic clusters analyzed in this study, and highlighting the areas that were affected by OXT neuronal ablation at 4-6 days-old: PrT, PT and posterior tuberal nucleus (PTN). Bottom*:* Quantification of TH cell density (cells/mm^2; mean of five sampled slices for each area, see Methods section for details) in brains of adult fish untreated (NTR+, MTZ-) or MTZ-treated a 4-6 days-old (NTR+, MTZ+). Dopaminergic groups are named according to [59,60]. (C) OXT neuron-specific labeling of synapses: *oxt*:Gal4 drives the expression of the EGFP-fused synaptic vesicle marker synaptophysin-B in oxytocinergic synapses. (D) Schematic of a sagittal larva brain highlighting OXT neuronal projections (in magenta) to pretectal and posterior tuberculum dopaminergic clusters (in blue). (E, F) Representative example showing that the synaptic marker line synaptophysin-GFP (SY-GFP, green), driven under the OXT promoter, reveals bona fide OXT synapses containing the OXT peptide (anti-OXT, magenta) on TH positive cells (cyan) in both (E) pretectum and (F) posterior tuberculum clusters.

CE, cerebellar plate; *D*, dorsal telencephalon; *E*, epiphyysis; *OB*, olfactory bulb; *OT*, optic tectum; *PO*, preoptic area; *PrT*, pretectum; *TPd*, posterior tuberculum dorsal part; *PTh*, prethalamus; *TPv*, posterior tuberculum ventral part; *Teg*, tegmentum; *Th*, thalamus; *SP*, subpallium (includes Vv, Vd and Vs in adult); *Ppa*, anterior parvocellular preoptic nucleus; *VM*, ventromedial thalamic nucleus; *Vl*, ventrolateral thalamic nucleus; *PPp*, posterior parvocellular preoptic nucleus; *PTN*, posterior tuberal nucleus; *Hyp*, hypothalamus; *NTR*, nitroreductase; *MTZ*, Metronidazole.

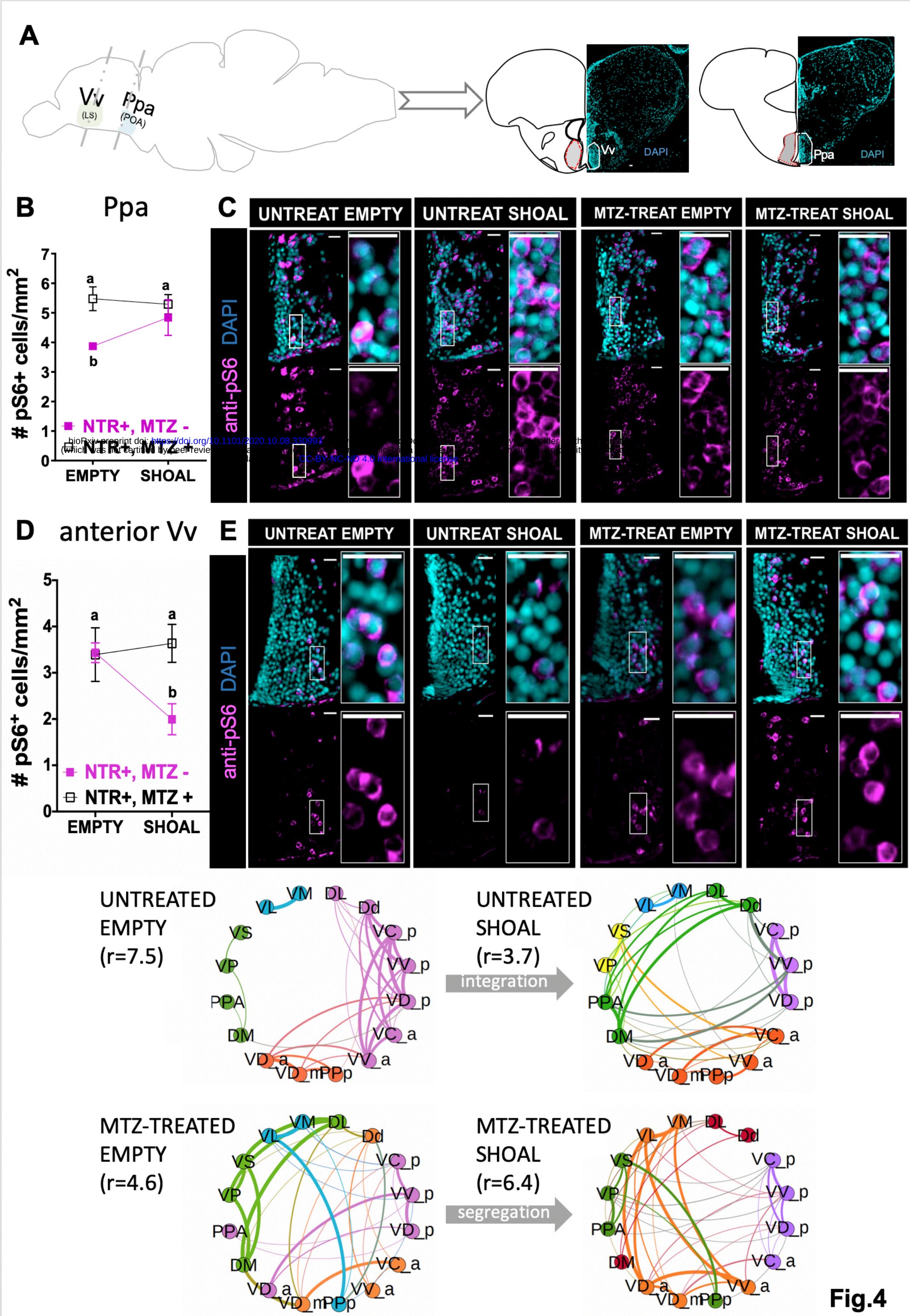

Fig.4

Figure 4. Early-life OXT shapes social information processing. (A) Anatomical localization of the two social responsive areas: anterior part of the ventral nucleus of the ventral telencephalon (Vv_a) and anterior part of the parvocellular preoptic nucleus (Ppa). Brain areas identified by DAPI. (B-E) Quantification of the density (cells/mm^2) of cells expressing the neuronal marker pS6 in 4-6 days-old MTZ-treated (open squares) or untreated adult fish (full squares), after exposure to either a shoal of conspecifics or an empty tank for 10 min in the Ppa area (B) and anterior Vv area (D) and respective representative examples (C, E). Scale: 20 μm. Data presented as mean ± SEM. (F) Changes in the modular structure of functional connectivity. Modules were obtained by extracting central partition from 400 optimization of Leiden algorithm [44] on the treatment correlation matrices. Node color indicates community membership. For visualisation purposes, we only show links with correlation weight >0.1. $\boldsymbol{r}$ values indicate the ratio of total edge weight within and between modules. High (low) values of $\boldsymbol{r}$ indicate more (less) segregated modular structure.

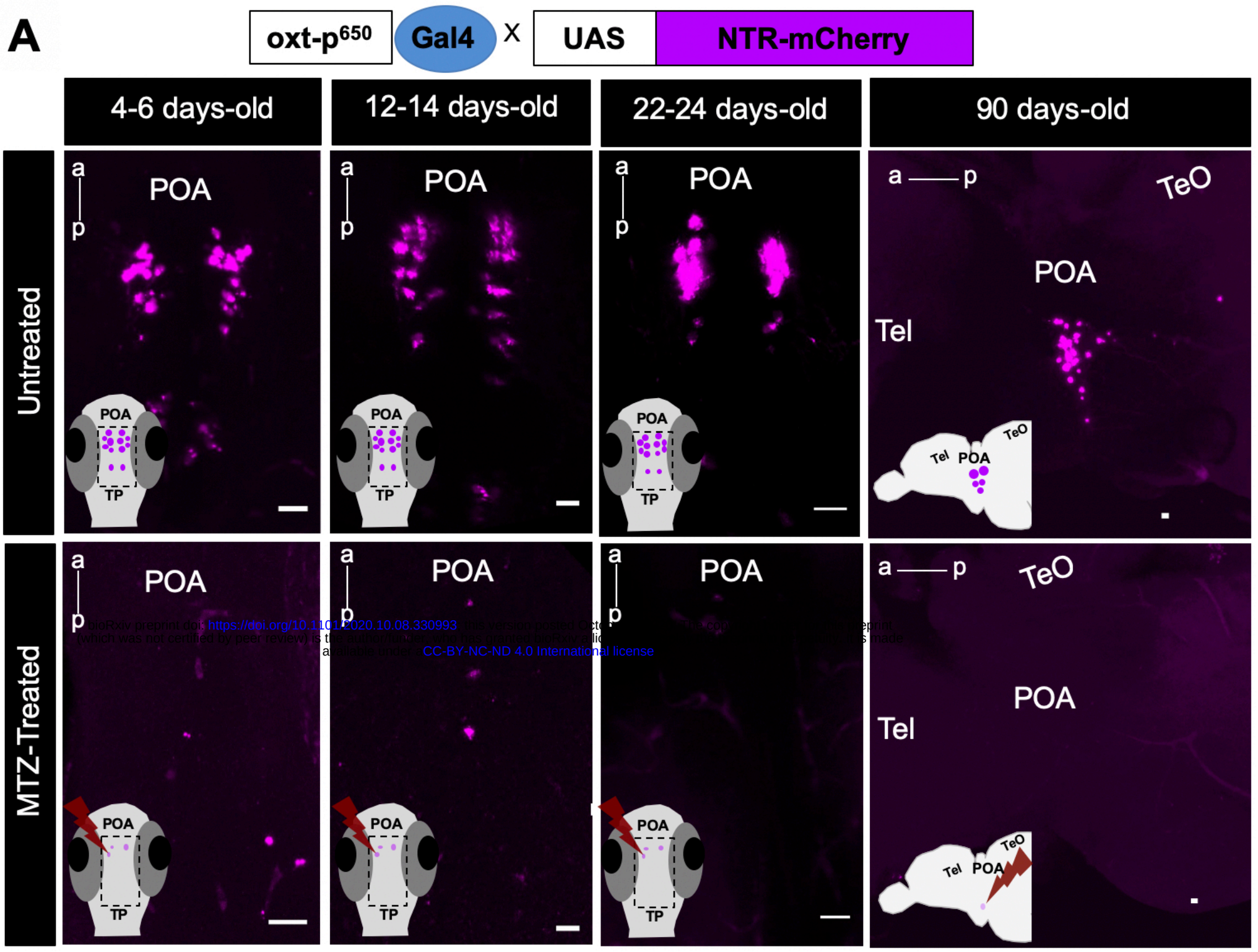

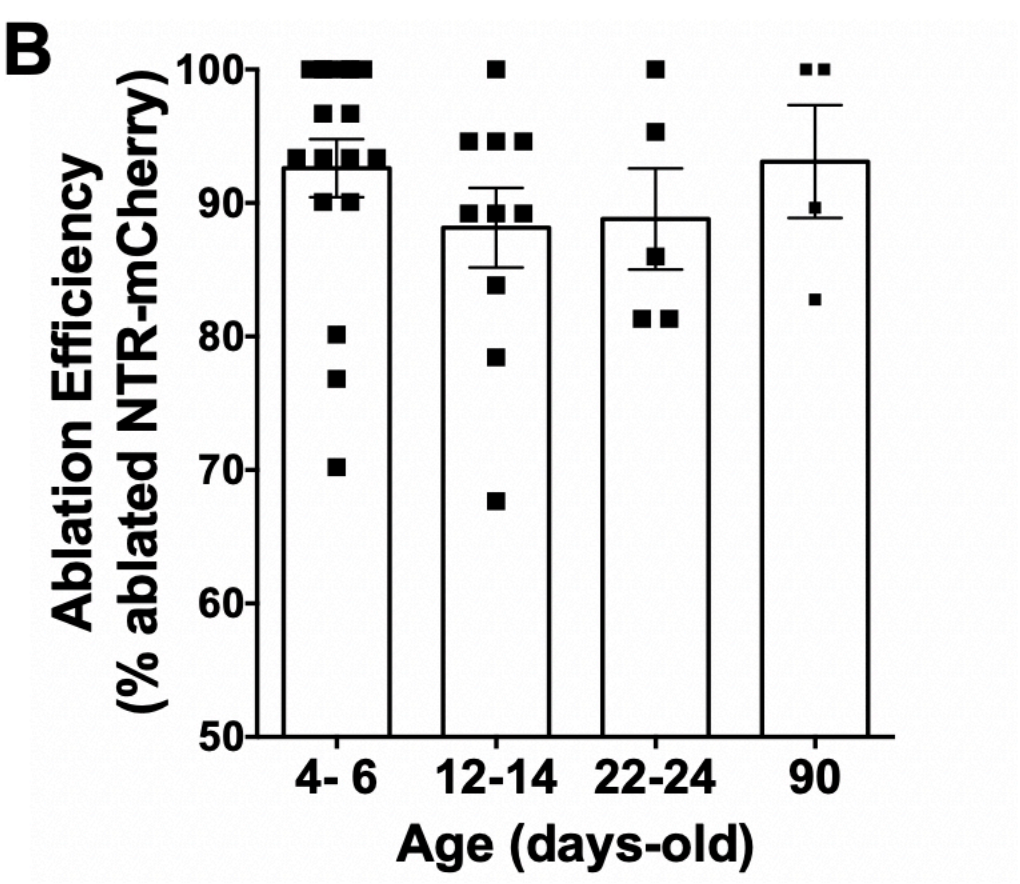

Fig. S1-related to Fig. 2

Figure S1-Related to Figure 2- Spatio-temporal control of OXT-specific transgene expression. (A) Representative example of the MTZ-treatment effect on transgene (*oxt*:GAL4/UAS-NTR-mCherry) at different treatment time-points. For 4-6, 12-14 and 22-24 days-old: whole mount larvae, maximum intensity confocal z-stack image, dorsal view, anterior to top; for 90 days-old: sagittal brain slice, maximum intensity confocal z-stack image, anterior to left. Scale: 20 μm. (B) Quantification of the effect of MTZ treatment on transgene expression at all ages tested (4-6 days-old, n=17; 12-14, n=10; 22-24 days-old, n=5; 90 days-old, n=4). Ablation efficiency was measured as percentage of ablated cells in MTZ-treated fish over mean number of NTR-mcherry cells in untreated fish. *NPO*, neurosecretory preoptic area; *Tel*, Telencephalon; *TeO*, tectum optic.

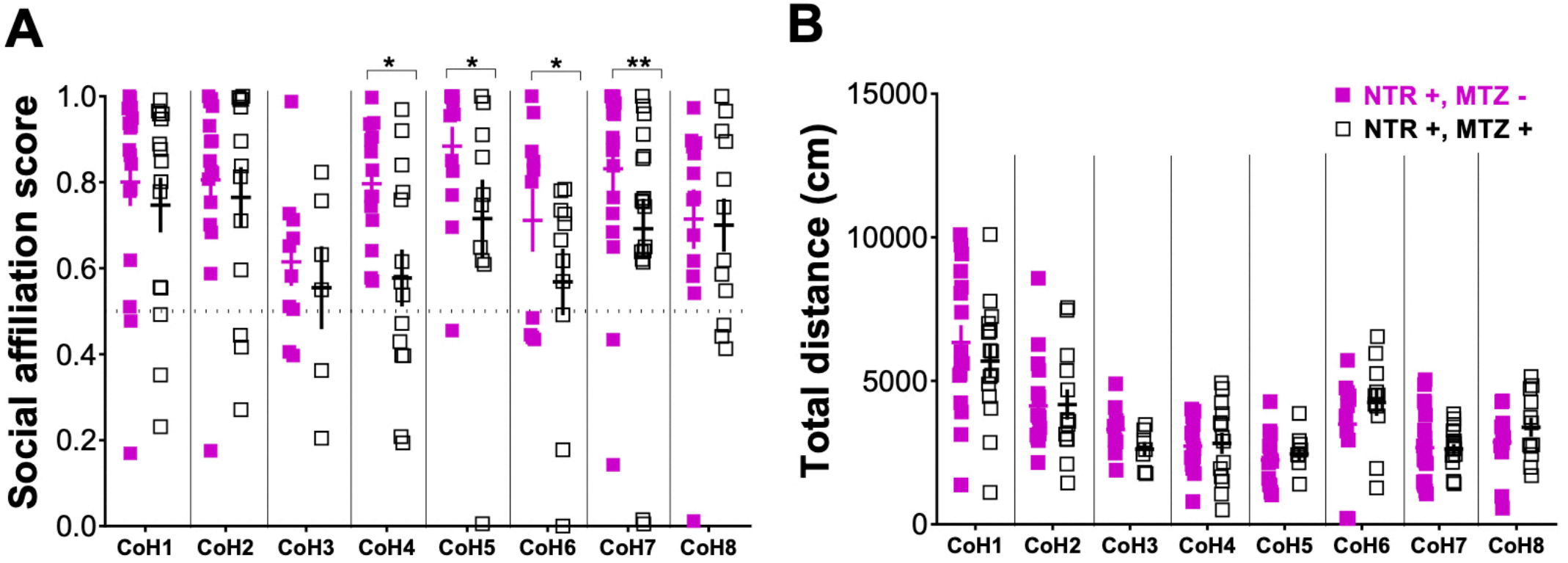

Fig S2- related to Fig.2

Figure S2. Related to Figure 2. Organizational vs activational effects of oxytocin neurons in adult social affiliation. Effect of early (4-6 days-old) MTZ treatment on (A) adult social affiliation; (B) total distance moved of eight independent cohorts of either MTZ treated at 4-6 days-old (NTR+, MTZ+) or untreated control fish (NTR+, MTZ-); (C) adult social affiliation and (D) total distance moved of control cohorts not expressing the transgene, 4-6 days-old MTZ-treated (NTR-, MTZ+) or untreated (NTR-, MTZ-). One-tailed p-values were considered in (A) because of our *a priori* directionality hypothesis that by ablating OXT neurons, MTZ treatment of fish expressing NTR transgene would decrease social affiliation behavior. Data are presented as mean ± SEM. Full squares (purple or dark gray): untreated fish (MTZ-); open square or light gray: MTZ-treated fish (MTZ+).

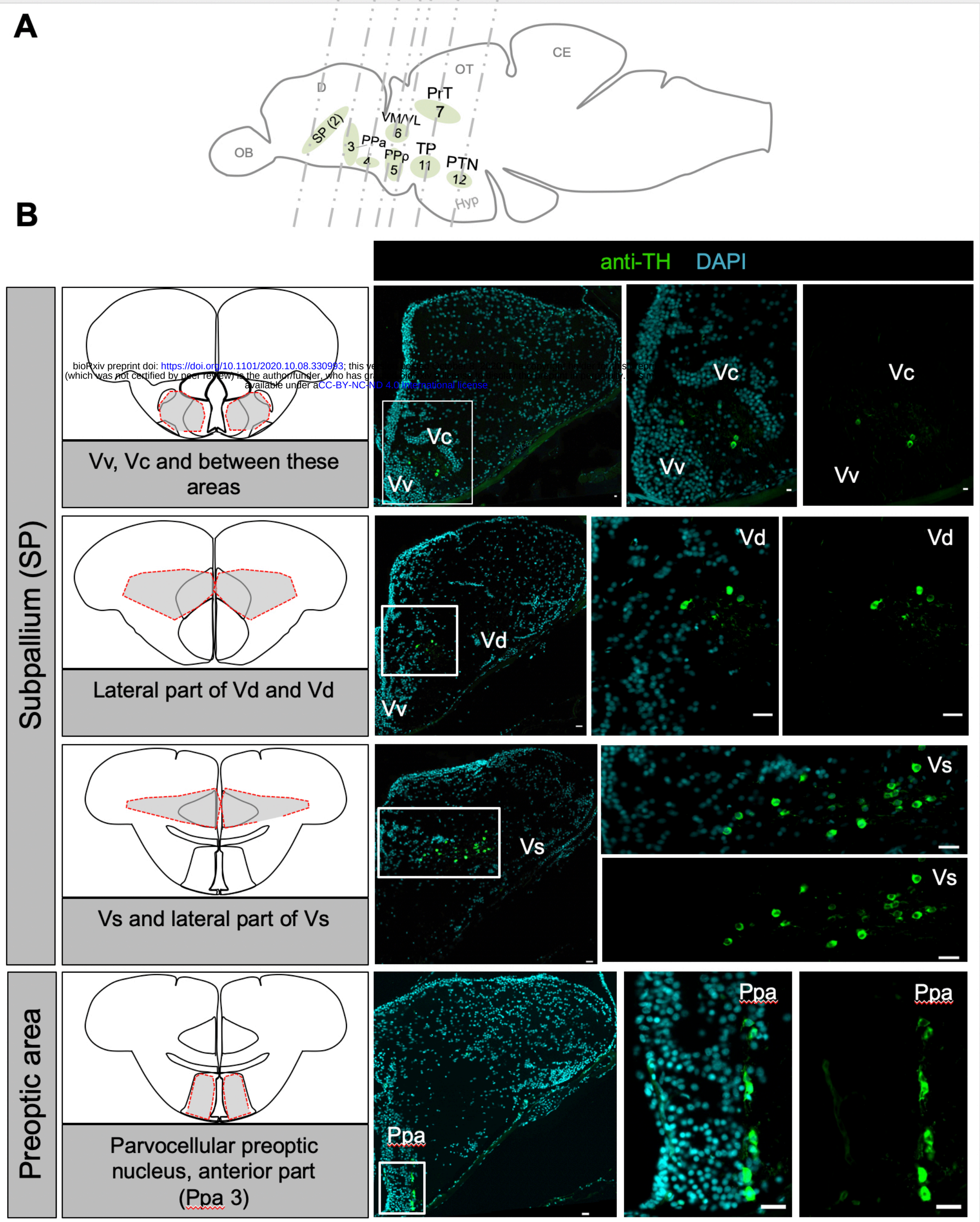

Fig. S3- related to Fig.3

anti-TH DAPI

Preoptic area

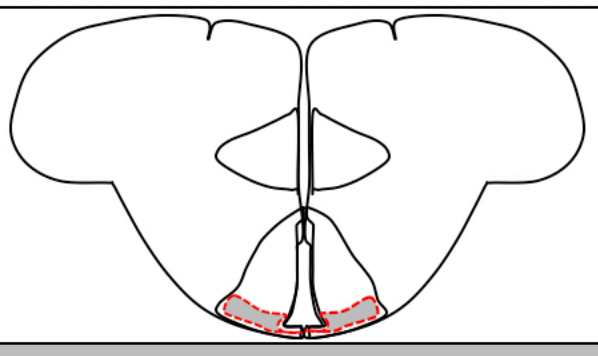

Parvocellular preoptic nucleus, anterior part (Ppa 4)

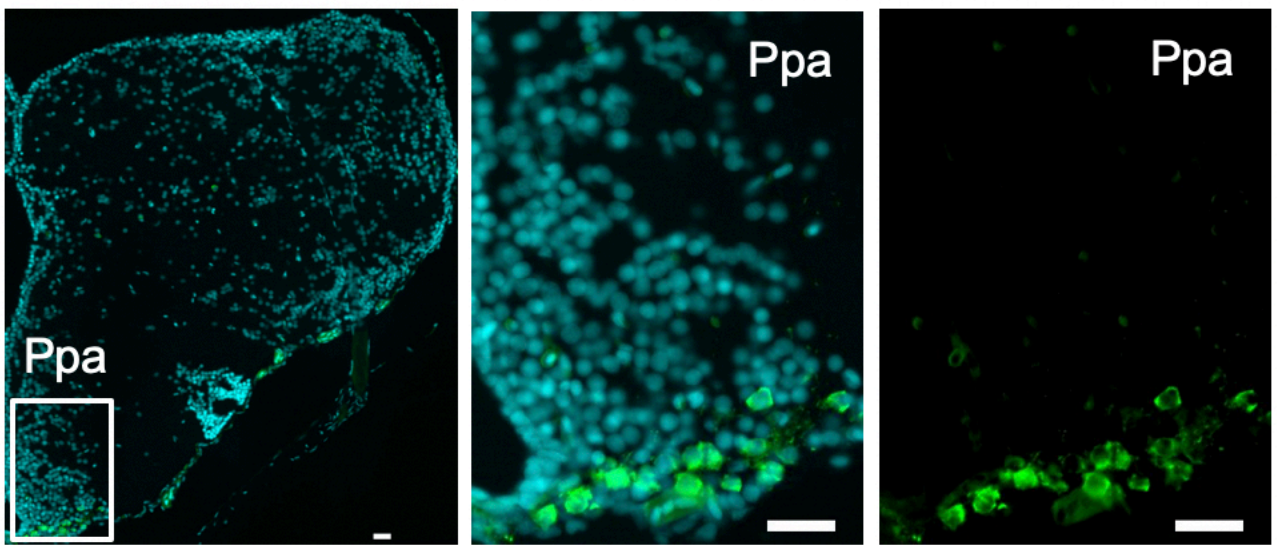

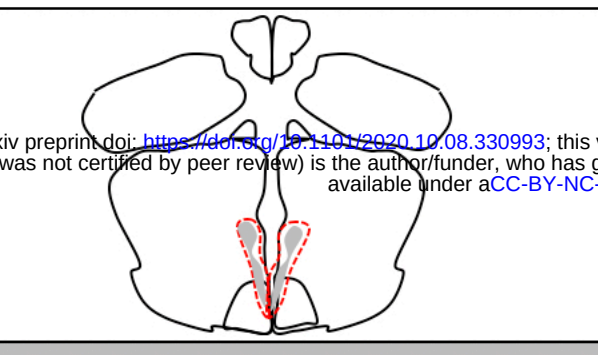

Parvocellular preoptic nucleus, posterior part (Ppp 5)

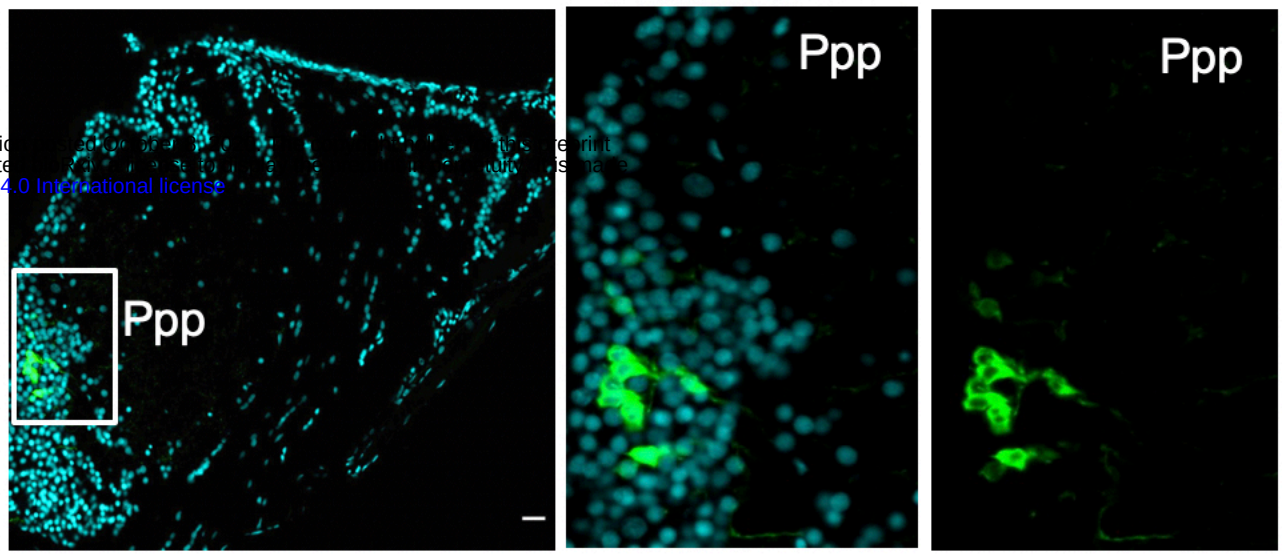

Thalamic area

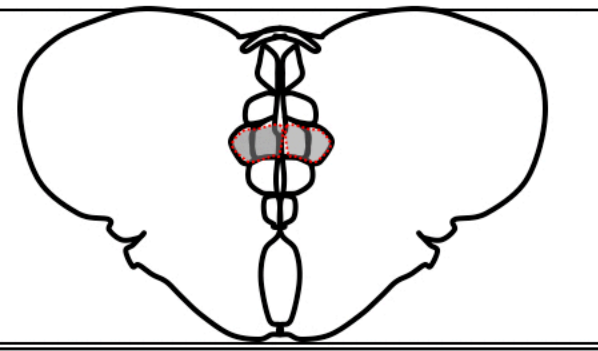

Ventromedial and ventrolateral thalamic nucleus (VM, Vl, 6)

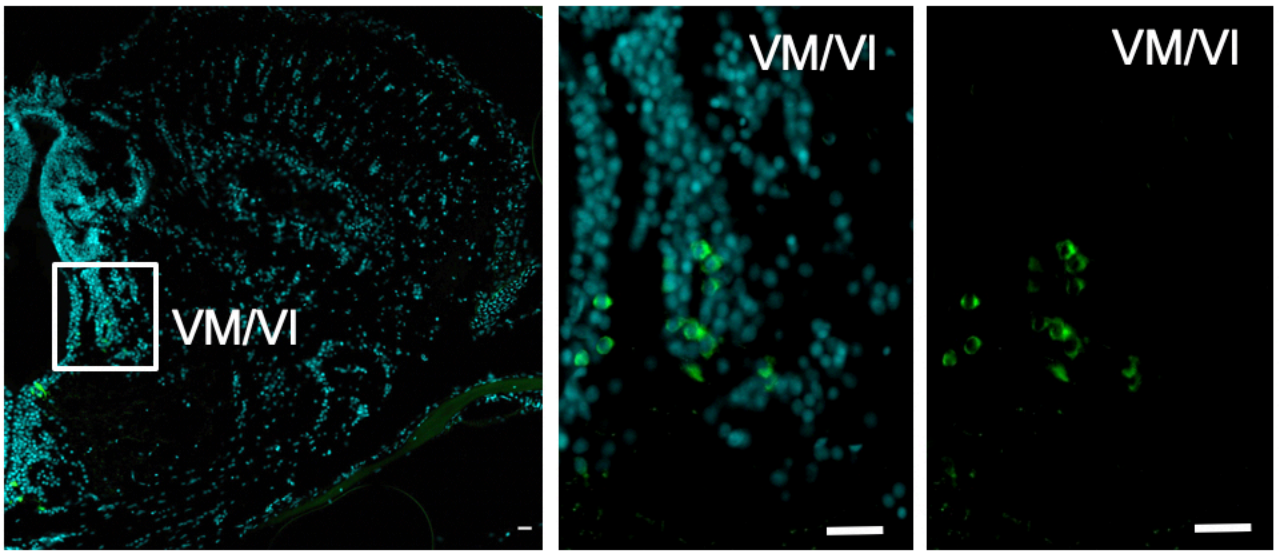

Pretectal area

Periventricular pretectal nucleus, (PrT, 7)

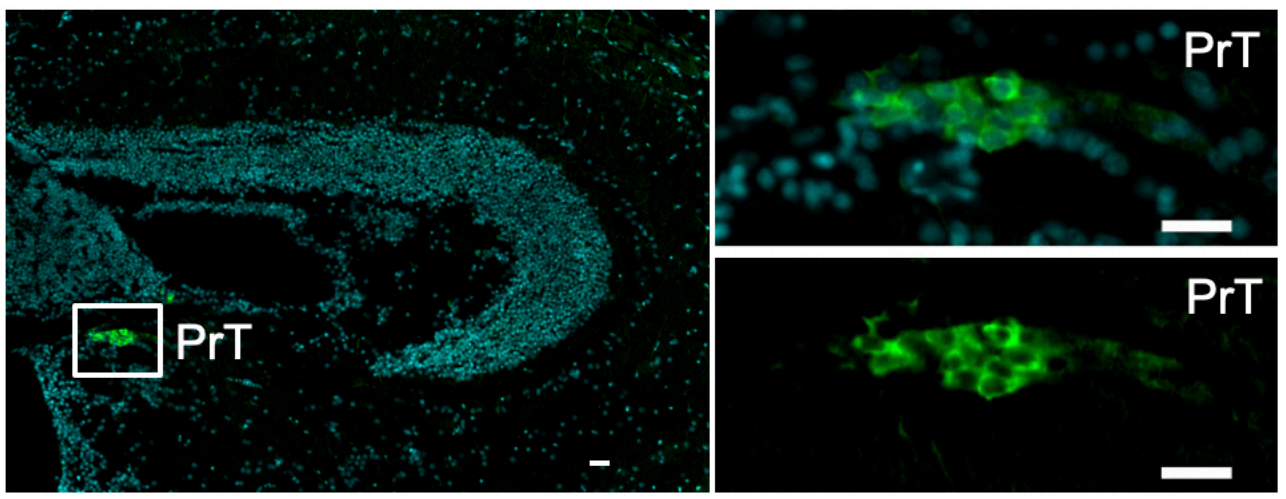

P. Tuberculum

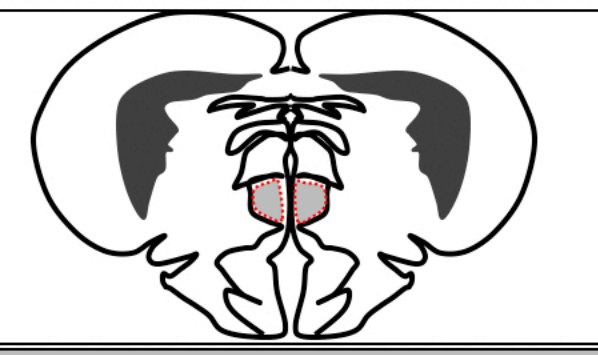

Periventricular nucleus of posterior tuberculum (TP,11)

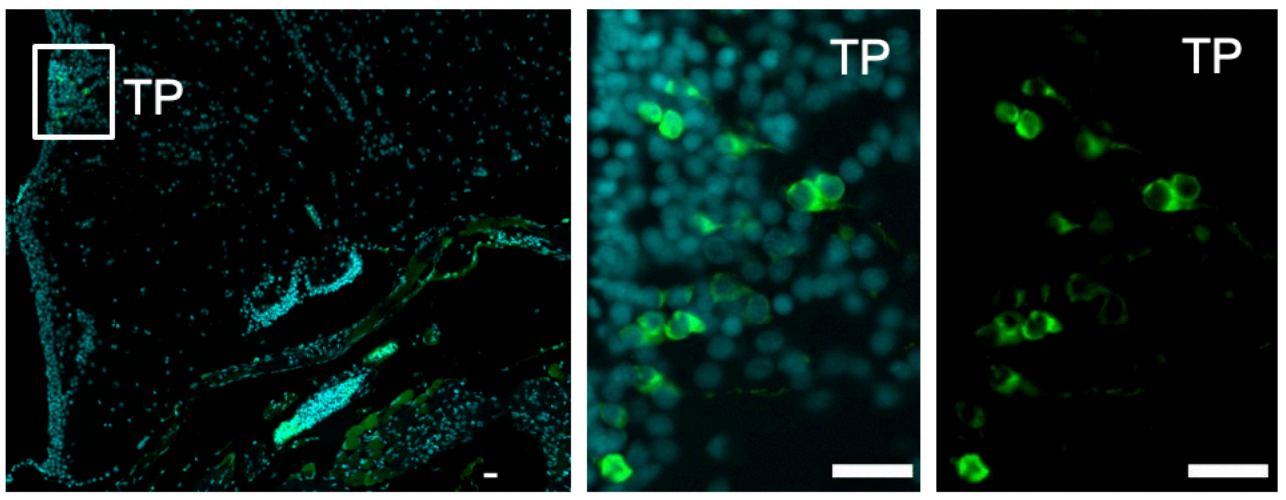

Fig. S3 (cont.)- related to Fig.3

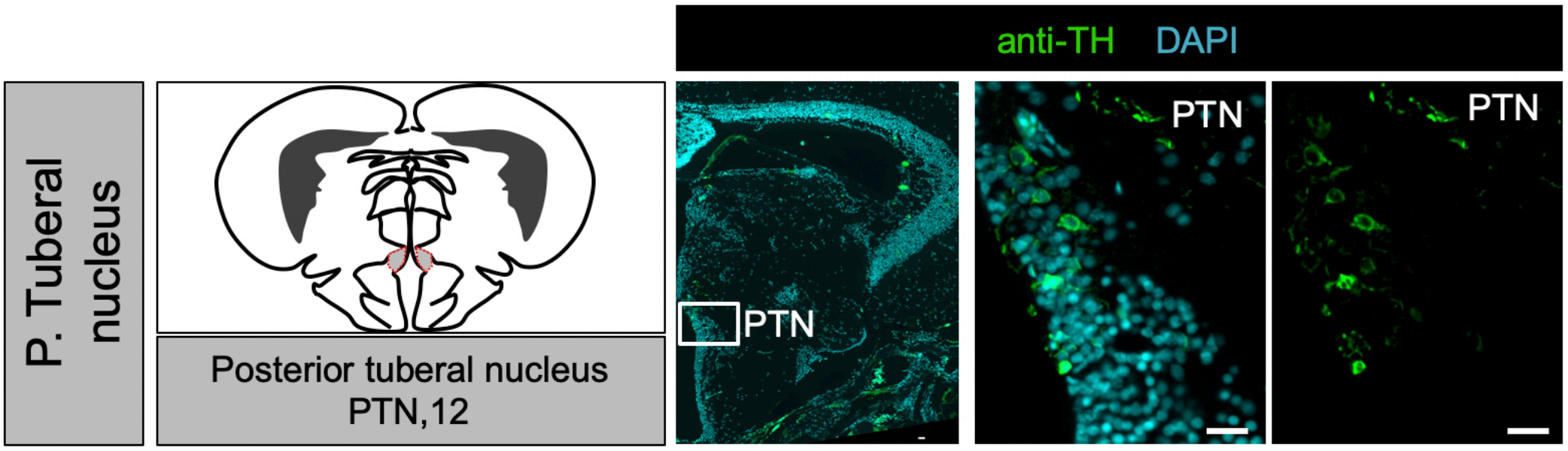

Fig. S3 (cont.)- related to Fig.3

Figure S3. Related to Figure 3. Early life OXT ablation affects the dopaminergic system. (A) Schematic representation of an adult zebrafish sagittal view representing the coronal sections of all dopaminergic areas sampled in the adult brain (dopaminergic cluster nomenclature accordingly to[60]). (B) Schematic representation of zebrafish brain coronal sections highlighting the different dopaminergic clusters (adapted from [70]) and representative example showing anatomical localization of the dopaminergic groups in an untreated adult zebrafish. Landmarks of the areas identified by DAPI (cyan) and dopaminergic groups by TH (Tyrosine Hydroxylase) immunostaining (green). Scale bars are 20μm.

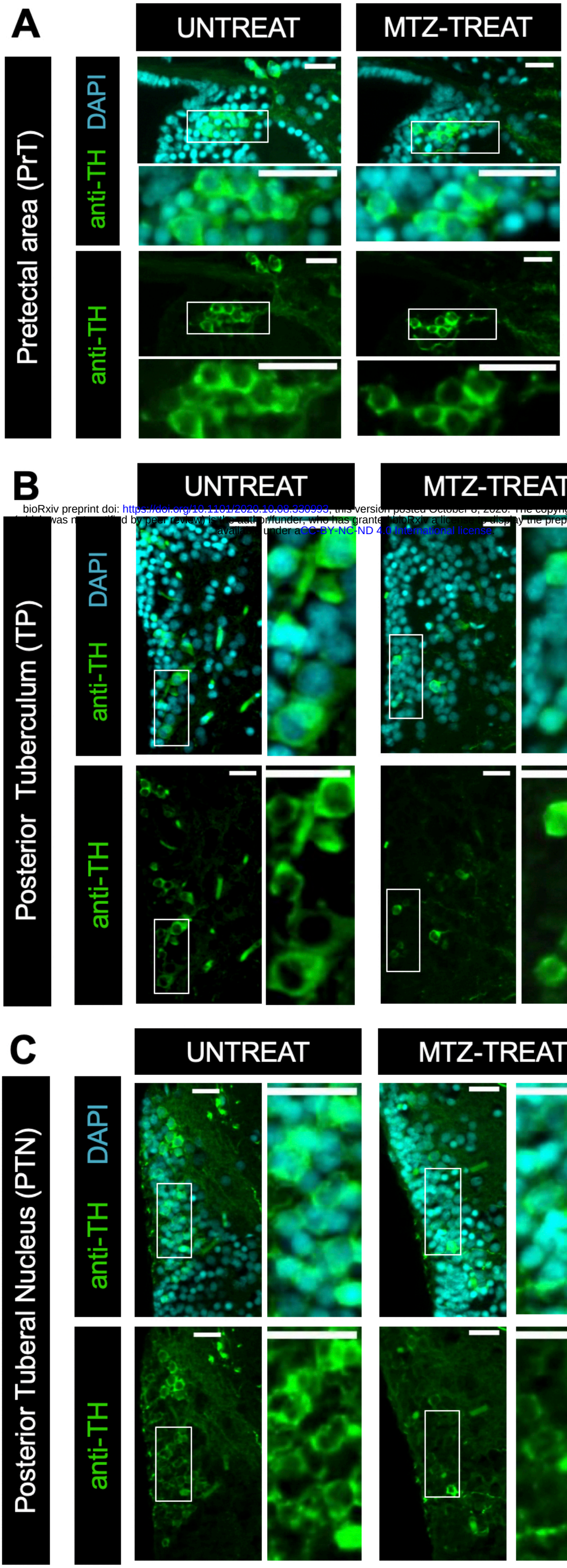

Fig. S4- related to Fig.3

Figure S4. Related to Figure 3. Early-life OXT ablation affects the dopaminergic system. Representative examples of the three adult brain TH-positive clusters that were altered by early OXT ablation (4-6 days-old MTZ treatment): (A) pretectal area, (B) posterior tuberculum and (C) posterior tuberal nucleus. Analyzed brain areas were identified by DAPI (cyan) and dopaminergic groups by TH (tyrosine hydroxylase) immunostaining (green). Scale: 20 µm.

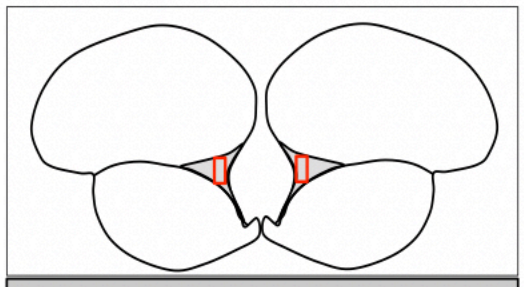

Dorsal nucleus of the ventral telencephalic area (anterior) Vd_a

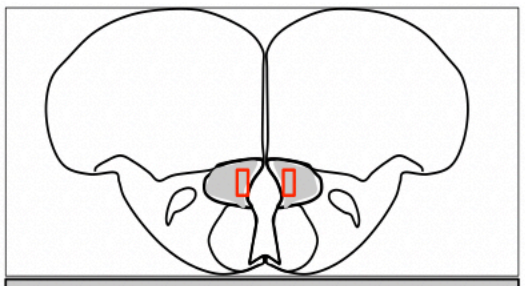

Dorsal nucleus of the ventral telencephalic area (medial) Vd_m

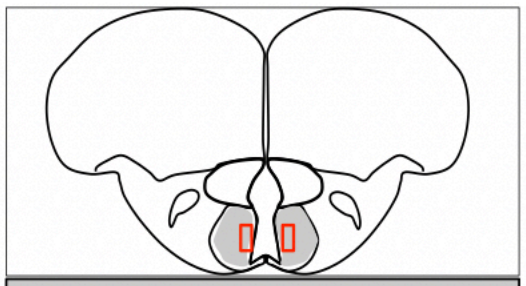

Ventral nucleus of the ventral telencephalic area (anterior) Vv_a

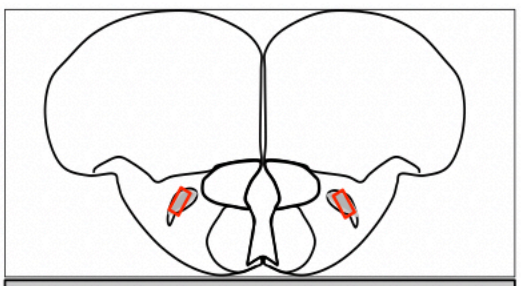

Central nucleus of the ventral telencephalic area (anterior) Vc_a

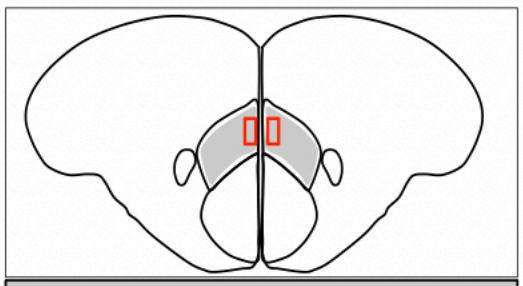

Dorsal nucleus of the ventral telencephalic area(posterior) Vd_p

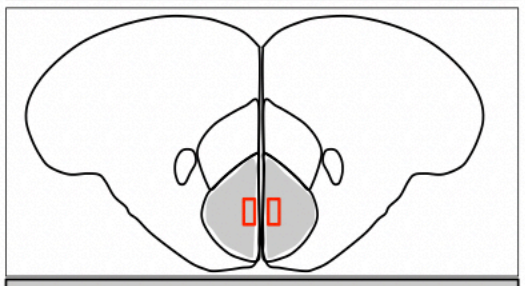

Ventral nucleus of the ventral telencephalic area(posterior) Vv_p

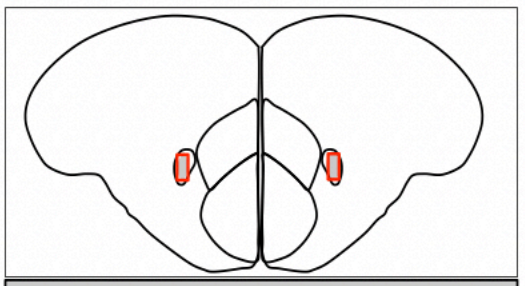

Central nucleus of the ventral telencephalic area(posterior) Vc_p

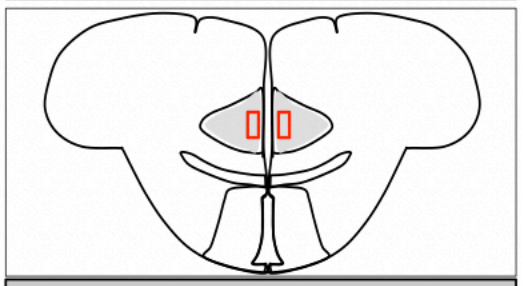

Supracommissural nucleus of the ventral telencephalic area, Vs

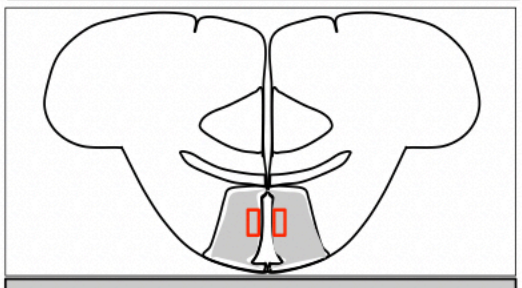

Parvocellular preoptic nucleus, anterior part, Ppa

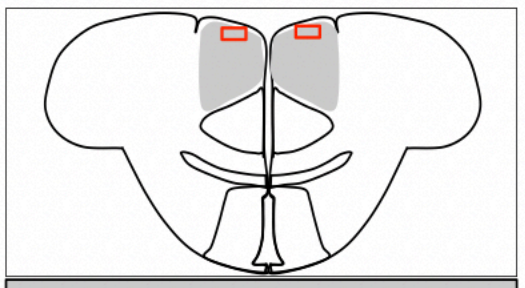

Medial part of the Dorsal telencephalic area, Dm

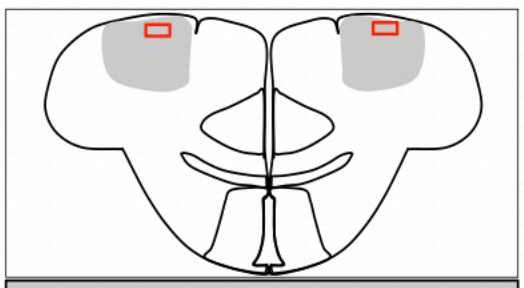

Dorsal part of the Dorsal telencephalic area, Dd

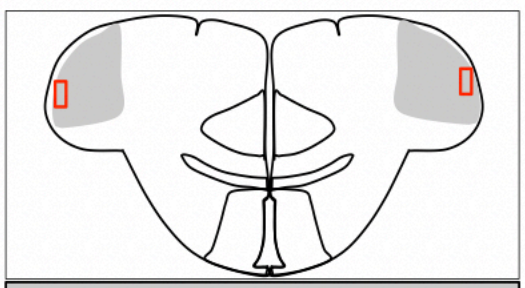

Lateral part of the Dorsal telencephalic area, Dl

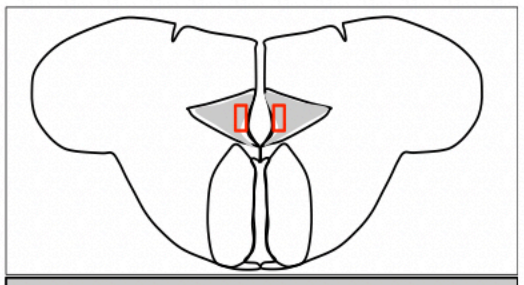

Postcommissural nucleus of the ventral telencephalic area, Vp

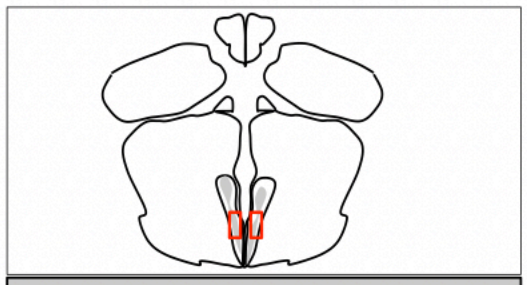

Parvocellular preoptic nucleus, posterior part, Ppp

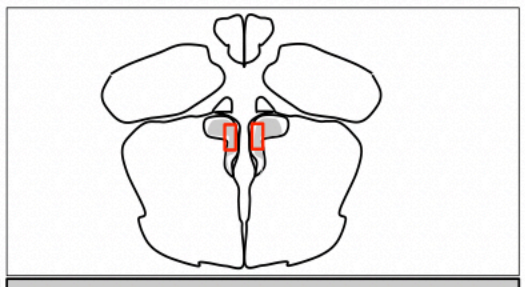

Ventromedial thalamic nucleus Vm

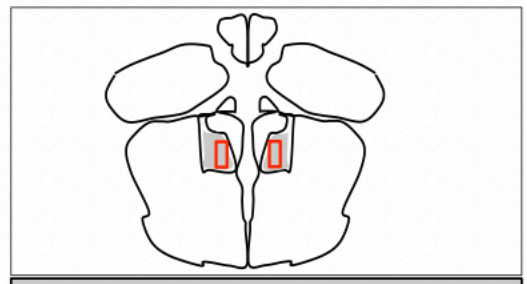

Ventrolateral thalamic nucleus Vl

Fig. S5- related to Fig.4

Figure S5. Related to Figure 4. Schematic representation of brain areas that were analyzed for neuronal activation in response to social stimulus. pS6 immunostaining served as a readout of neuronal activation following MTZ treatment at 4-6 days-old or untreated adult fish to either a shoal of conspecifics or an empty tank. Included brain areas are part of the social decision-making network, subdivided into more anterior or posterior parts. Schematics are adapted from zebrafish atlas [70].

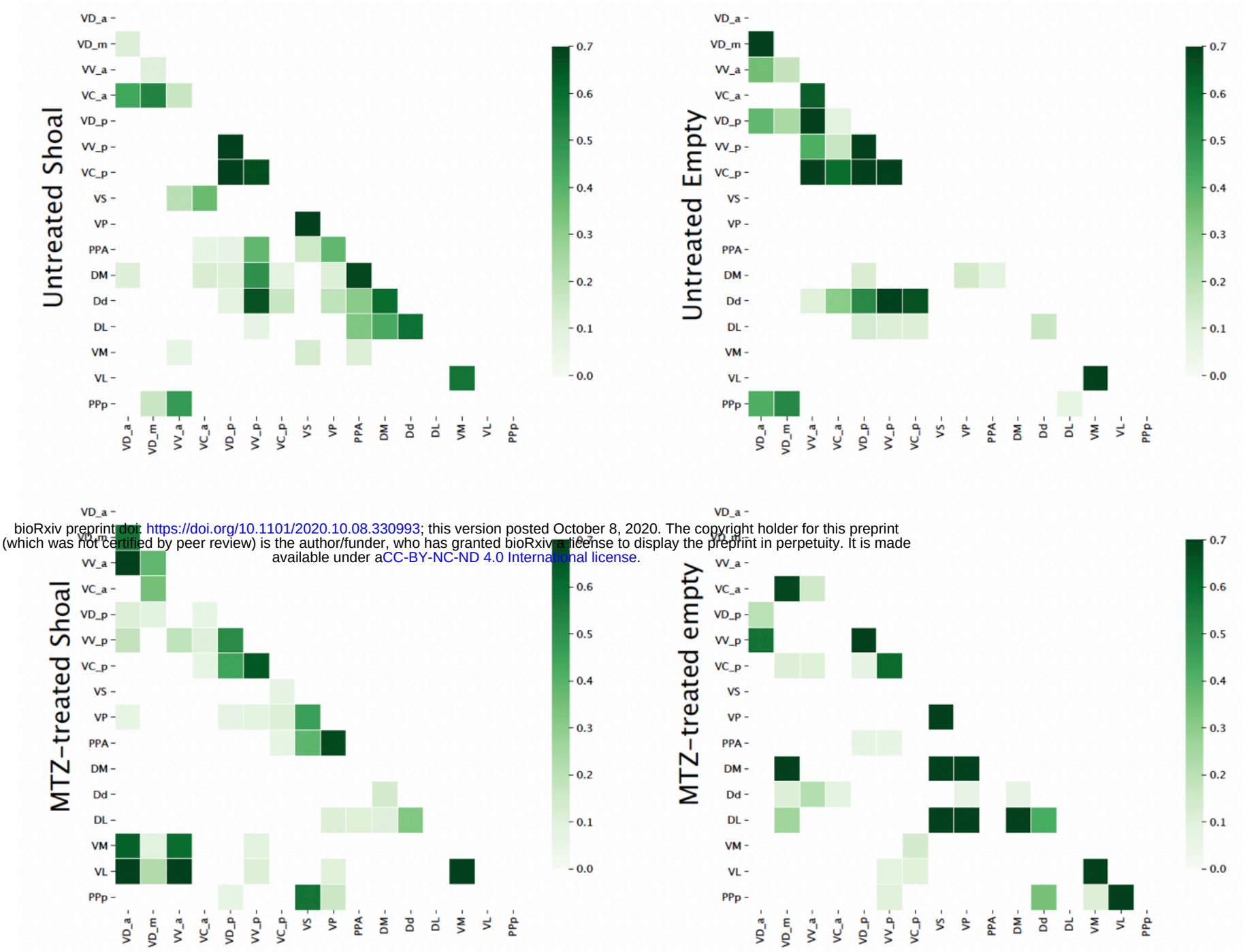

Fig. S6-Related to Fig.4

Figure S6. Related to Figure 4. Correlation matrices of functional connectivity for the four treatments reveal early-life OXT shapes social information processing. Regional correlation values are computed joining data from both hemispheres. Resampled correlations were kept if significant ($p<0.05$). For visualisation purposes, we show only entries of significant correlations higher than 0.05. Label legend: CE, untreated empty; CS, untreated shoal; AE, MTZ-treated empty; AS: MTZ-treated shoal.

STAR METHODS

KEY RESOURCES TABLE

REAGENT or RESOURCE	SOURCE	IDENTIFIER
Antibodies		
Rabbit monoclonal anti-phospho-S6 ribosomal protein (Ser235/236) (D57.2.2E)XP	Cell Signaling Technology	CAT# 1674858S
Chicken polyclonal anti-GFP IgY Antibody Fraction	Life Technologies	CAT# A10262
Mouse monoclonal anti-Tyrosine hydroxylase, clone LNC1	Merck Millipore	CAT# MAB318
Rabbit polyclonal anti-GFP	ThermoFisher	CAT# A-11122
Guinea pig polyclonal anti-oxytocin	Peninsula labs	CAT# T-5021
Alexa 488 or 594 secondary antibodies	Molecular Probes	CAT# A-11008, A-11001, A-11012
Fast red tablets	Roche	CAT # 11496549001
Chemicals, Peptides, and Recombinant Proteins		
Metronidazol Vetranal	Sial	CAT#46461-250MG
2-Methyl-5-nitroimidazole-1-ethanol	TCI Europe	CAT#M0924-25G
Metronidazol Veterinary preparation	Vetmarket; POB- 960, Shoham, Israel	CAT#165228
Vectashield mounting medium with DAPI	Vector Laboratories, Burlingame, CA	CAT#H-1500
EverBrite™ Hardset Mounting Medium	Biotium	CAT#23003
Aqua-Polymount	Polysciences, Inc, Warrington, PA	CAT#18606-20
Critical Commercial Assays		
Deposited Data		
Experimental Models: Organisms/Strains		
Tg(*oxt*:gal4)wz06	(Anbalagan et al., 2018)[61]	ZDB-ALT-171113–2
Tg(UAS:NTR-mCherry)c264	(Davison et al., 2007)[62]	ZDB-ALT-070316–1
Tg(*oxt*:EGFP)wz01	(Blechman et al., 2011)[63]	ZDB-ALT-111103–1
Tg(UAS:sypb-GFP)	(Meyer &Smith, 2006)[64]	ZDB-TGCONSTRCT-150601-1
Software and Algorithms		
Ethovision XT 11.5	Noldus Technology	www.noldus.com/ethovision
Imagej	Schindelin, J. et al 2012 [65]	http://imagej.nih.gov.ij/ RRID:SCR_003070
GraphPad Prism version 6.0c	GraphPad software, San Diego, California, USA	www.graphpad.com
R	R Development Core Team (2019).	http://www.r-project.org/index.html
Others		

Nikon High Content Screening microscope with a Andor Zyla 4.2 sCMOS camera, 100X 1.45 NA objective, DAPI + GFP fluorescence filtersets and controlled with the Nikon Elements software	Nikon	
Zeiss LSM 800 confocal scanning microscope with a 20X M27 Plan ApoChromat air objective. Pixel size was 0.156X0.156X0.96 uM (x*y*z).	Zeiss	
SlideScanner Zeiss AxioScan Z1	Zeiss	
High speed camera FLARE 2M360	Io Industries	
B&W mini surveillance camera	Henelec 300B	

Experimental model

Zebrafish were raised and bred according to standard protocols. All experimental procedures were conducted in accordance with standard operating procedures of the Instituto Gulbenkian de Ciência and Direcção Geral de Alimentação e Veterinária (DGAV), Portugal, and Institutional Animal Care and Use Committee (IACUC) of the Weizmann Institute, Israel.

Zebrafish transgenic/mutant lines used in this study: Tg(oxt:EGFP)[63], Tg(*oxt*:gal4)wz06 [61], Tg(UAS:NTR-mCherry)c264 [62], Tg(UAS:sypb-EGFP) [64].

Larvae and adult zebrafish (3-6 months old) of both sexes were used in this work.

Social affiliation assay

The social preference test followed the protocol described previously [10,22]. Briefly, focal zebrafish were given a choice between two side-by-side compartments: one containing a shoal (two males and two females) and an empty one (Figure1A, B) during a 10-min test. The stimulus shoal matched the genotype of the focal fish. The stimulus compartment was randomly switched between tests, to control for any place preference possibly induced by the arena or laboratory frames. All compartments were completely sealed to block transmission of chemical and vibrational stimuli and thus, only visual cues were accessible. The experimental test tank was placed over a custom-built infrared LED light box, to increase image quality for subsequent automated video tracking. Fish behavior was recorded from above with either a high-speed camera FLARE (2M360, Io Industries) or a B&W mini surveillance camera (Henelec 300B) connected to a computer, using video recording software (Pinnacle Studio 12). Videos were analyzed with Ethovision XT11.0 (Noldus Inc., The Netherlands). Relevant data were then exported and further analyzed. The two regions of interest, empty and shoal, were defined as the 1/10 of the length of the arena immediately adjacent to the empty compartment or the compartment containing the stimulus shoal, respectively. The percentage of cumulative time fish spent these regions of interest ($\%T_{shoal}$ and $\%T_{empty}$) was used to calculate the social affiliation score [$\%T_{shoal}/(\%T_{shoal} + \%T_{empty})$]. This score, also called the sociability score, has been commonly used in rodent studies to measure sociability in the 3-chamber test [33]. Total distance traveled was also measured.

Ontogeny of social affiliation behavior: Social preference was tested at different developmental stages: early larvae (12 days-old), mid larvae (14-20 days-old), post-flexion metalarvae (21-30 days-old), juveniles and adults (from 30 to 90 days-old). The size of the testing arena for early larvae was 3.5 x 6.0 cm; for mid larvae 7.0 x 8.0 cm; for metalarvae 7.0 x 10.0 cm; and for juveniles and adults it was 20.0 X 20.0 cm. The stimulus shoal matched the developmental stage of the focal fish. Two different experiments were performed: a) longitudinal, where individual fish were repeatedly tested at each developmental time point, and b) cross-sectional, where individual fish were tested only once, at a given developmental time point.

Chemo-genetic oxytocinergic ablation

Early ablation: Nitroreductase (NTR)-mediated cellular chemo-genetic ablation was conducted as previously described[18,19]. Briefly, larvae (~30-40 per petri dish) were treated with metronidazole (MTZ, Vetranal CAT#46461, Sigma) dissolved in Danien's buffer to a final concentration of 10mM for 48 h while being protected from light, to prevent MTZ photoinactivation. After the first 24 h, the MTZ-containing Danien´s buffer was replaced by fresh MTZ medium. Control untreated larvae were subjected to the same procedure in Danien´s buffer without MTZ, but were also protected from light. After 48 h of treatment, larvae were washed out several times in Danien´s buffer.

Adult ablation: We used a modified ablation protocol of 3X48 h MTZ treatments (5 mM), as we observed that this increased survival of adult animals. Briefly, adult zebrafish were placed into 2-liter tanks containing MTZ (Veterinary preparation, Vetmarket; Shoham, Israel, CAT#165228, or 2-methyl-5-nitroimidazole-1-ethanol, TCL Europe, CAT#M0924) dissolved in system water at a final concentration of 5 mM, protected from light. After ~16 h of treatment, zebrafish were moved to a tank containing fresh system water without MTZ, fed, and allowed to recover for ~2 h, followed by a second treatment of MTZ 5mM for 16 h. Animals were then allowed to recover in their home tanks for 48 h. The entire protocol was repeated three times.

Effect of chemo-genetic oxytocinergic ablation on endogenous OXT cells. Zebrafish treated with MTZ at different time points during development (4-6 days-old, 12-14 days-

old, 20-22 days-old or 90 days-old) were allowed to recover from treatment for 48 h and were then sacrificed to assess the treatment effects on endogenous OXT cells by *in situ* hybridization (see below) or by direct visualization of the mCherry transgene signal.

Effect of chemo-genetic oxytocinergic ablation on adult social affiliation. Zebrafish treated with MTZ at 4-6 days-old, 12-14 days-old, 20-22 days-old or 90 days-old were allowed to grow until adulthood to be tested for social affiliation behavior (see above).

Effect of 4-6 days-old chemo-genetic oxytocinergic ablation on adult neuronal activity (pS6 activation). To assess the effect of early OXT ablation on adult brain activation patterns in response to a social stimulus, adult zebrafish that had been treated with MTZ at 4-6 days-old and untreated controls were exposed individually to either a mixed-sex shoal of conspecifics or an empty tank for 10 min. Immediately after, we blocked the visual stimulus, without disturbing the focal fish, by placing an opaque partition between the experimental and stimulus tanks. After 50 min (to allow for expression of the pS6 neural activation marker), zebrafish were sacrificed and heads were collected and processed for paraffin slice immunofluorescence (see below).

Effect of 4-6 days-old chemo-genetic oxytocinergic ablation on larvae and adult dopaminergic system. Untreated and 4-6 days-old MTZ-treated zebrafish larvae were allowed to recover from treatment (48h) and were either processed immediately for whole-mount larvae TH immunofluorescence (see below) or allowed to grow until adulthood and then processed for paraffin slice TH-immunofluorescence (See below).

In situ hybridization

RNA *in situ* hybridization was performed on both whole larvae and whole adult brains. Larvae or dissected brains were fixed in 4%PFA and *in situ* hybridization was performed as described in [22,66]. An OXT probe was generated using a pGEM plasmid encoding for *oxt* mRNA (RefSeq NM_178291.2). Following development with Fast Red reagent (Roche, cat. No. 11496549001), adult brains were embedded in agar and sagittally cut at a thickness of 150µm on a vibratome, and whole larvae and brain slices were mounted in glycerol and imaged on a Zeiss LSM 800 scanning confocal microscope.

Whole-mount larvae immunofluorescence

Briefly, larvae were euthanized in ice-cold water, transferred to 4% PFA and then incubated overnight at 4°C on a shaker. Then, the PFA was washed out and samples were placed in pre-cooled acetone in a freezer at -20°C for 10 min. The acetone was washed out (PBS 0.1% TritonX-100), and the samples were then incubated in blocking solution (PBS 0.1% triton + 1% DMSO + 1% BSA + 5% NGS) for minimum of 2 h at room temperature (RT), followed by incubation with primary antibody overnight at 4ºC on a shaker. Primary antibodies used were either mouse anti-TH (MAB 318, Merck Millipore), rabbit anti-EGFP (A11122, ThermoFisher) or guinea pig anti-OXT (T-5021, Peninsula labs), at a concentration of 1:200. Next, samples were washed repeatedly (minimum of 6X15 min washes) with blocking solution and then placed in a blocking solution containing fluorescent secondary antibody overnight at 4ºC on a shaker. Then, samples were washed in PBS, mounted dorsally on a slide in mounting medium (Aqua-Polymount, Polysciences Inc., Warrington PA, CAT# 18606-20) and imaged by a Zeiss LSM 800 scanning confocal microscope.

Paraffin adult brain slice immunofluorescence

Zebrafish heads were fixed in 10% buffered formalin for 72 h and decalcified in EDTA (0.5 M, pH 8.0) for 48 h, followed by paraffin inclusion. Coronal slices (6 µm-thick) were cut with a microtome. Sectioned slices were then processed for immunofluorescence. After antigen retrieval with Tris-EDTA (10 mM Tris Base, 1 mM EDTA, 0.05% Tween20) at 95ºC for 20 min, slices were washed in TBS-Tx (TBS 0.025% TritonX-100, 3X10 min), then incubated with blocking solution (TBS 0.025% TritonX-100 + 1%BSA) for 1 h at RT, followed by an overnight incubation with a primary antibody (1:400 at 4ºC). Slides were then washed in TBS- 0.025% TritonX-100 (3X10 min) and incubated in secondary antibody (1:1000 for 2 h). After washes, slices were incubated with DAPI for 20 min, then rinsed in TBS and mounted with EverBrite™ Hardset Mounting medium (Biotium). Primary antibodies used were anti-phosphorylation of S6 ribosomal protein, pS6 (Cell signaling S235/236) and anti-tyrosine hydroxylase, anti-TH, (mouse monoclonal, MAB 318, Merck Millipore).

Neuronal quantifications

Neuronal pS6 cell quantification

Coronal slices were acquired with a commercial Nikon High Content Screening microscope, based on Nilon Ti equipped with a Andor Zyla 4.2 sCMOS camera, using a 20X 0.75 NA objective, quadruple dichroic filter, and controlled with the Nikon Elements software. To avoid double-imaging of the same cells, we imaged every other slice alternately. We quantified density of pS6-positive cells in 16 brain areas that belong to the social decision making network [39]: Vv- ventral nucleus of the ventral telencephalic area (V), homologous to the mammalian lateral septum, subdivided into: anterior (Vv_a) and posterior (Vv_p); Vd- dorsal nucleus of V, homologous to the mammalian Nacc, subdivided into: anterior (Vd_a), medial (Vd_m) and posterior (Vd_p); Vc- central nucleus of V, homologous to the mammalian striatum, subdivided into: anterior (Vc_a) and posterior (Vc_p); Dm- medial zone of the dorsal telencephalic area (D), homologous to the mammalian bLAMY; Dl- lateral zone of D, homologous to hippocampus; Dd- dorsal zone of D; Vs- supracommissural nucleus of V, homologous to the mammalian extended amygdala (BNST and meAMY); Vp- postcommissural nucleus of V; Ppa- parvocellular preoptic nucleus, anterior part and Ppp- parvocellular preoptic nucleus, posterior part, both homologous to the mammalian preoptic area; VM- ventromedial thalamic nucleus; VL-ventrolateral thalamic nucleus (Figure S3, related to Figure 3).

For each brain area, about five coronal brain slices were analyzed manually using imageJ software [65]. Background subtraction and linear adjustments of brightness and contrast levels were performed in the same way for all groups. The brain areas of interest were identified using DAPI to define neuroanatomical boundaries and landmarks identified in the Zebrafish Atlas [41]. In each brain slice, we placed one square of 1000 μm^2 in the brain region of interest, in each hemisphere, following these criteria: the square was always placed over the highest number of pS6-positive cells, keeping minimum distance from the border and edge of the brain section, a similar strategy that has been used by others [67]. pS6-positive cells were counted if a nucleus surrounded by the cytoplasm was clearly visible, and if the intensity of the pS6 signal was perceptibly greater than background (see Figure 3 and Figure S2B, related to Figure 3, for examples of pS6 staining in the sampled brain areas). To compare neuronal activation between treatments

and stimuli, we used a Generalized Linear Mixed Model (GLMM) with a Poisson distribution using the brain identification number as the mixed effect in the statistical model, followed by planned comparisons, since we target areas that are known to belong to the social decision-making network. We analyzed the 16 brain areas independently and corrected the p-values of the planned comparison with the false discovery rate (FDR) adjustment method.

Dopaminergic neuronal quantification

Dopaminergic quantification was performed in both larvae and adult zebrafish, either 4-6 days-old MTZ-treated or untreated. Briefly, for larvae, whole-mount zebrafish immunofluorescence was performed as described above using primary antibody anti-TH (MAB 318, Merck Millipore). Larvae were imaged and confocal z-stacks were analyzed by ImageJ. Larva dopaminergic forebrain, pretectum and posterior tuberculum nucleus were identified accordingly to [68,69] and TH+ cells were counted in these three groups. To compare dopaminergic cell numbers between treatments, and since the data were normally distributed, we used a Linear Model (LM) to analyze each brain area independently (Table S5).

For adults, heads from both treatment groups (untreated and 4-6 days-old MTZ-treated) were collected and processed for paraffin embedding, followed by paraffin slice immunofluorescence as described above. Coronal slices were acquired with a SlideScanner Zeiss AxioScan Z1 (Zeiss), and analyzed with Zeiss Zen Lite software. To avoid double-imaging of the same cells, we imaged every other slice alternately. Boundaries separating brain nuclei and subdivisions were identified based on DAPI staining, using as reference a coronal atlas of the zebrafish [70]. Dopaminergic cells were marked and counted if a nucleus surrounded by the cytoplasm was clearly visible, and if intensity of TH staining was perceptibly greater than background (see Figure S5, related to Figure 4, for examples of TH staining in the sampled brain areas).

Dopaminergic nuclei (TH^+) groups were identified according to [30,59,60]. We counted TH^+ cells in the following clusters: the subpallium area (extending from the rostroventral telencephalon to the dorsocaudal telencephalon, also identified by G2 by Panula and colleagues [60]), which included a TH cluster containing VV, Vc and Vl, and in-between

areas, a TH cluster including Vd and the lateral area outside the Vd, and a TH cluster within the Vs (identified by the anterior commissure) and lateral area outside the Vs; TH clusters in the PPa area were divided in two: a more anterior (close to the border of the diencephalon, lateral margin of the ventricle, G3) and a more extending area in the medial area of the PPa (ventral part of the PPa, G4); a TH cluster in the pretectum (PPr, G7); in the ventromedial and ventrolateral nucleus (Vm, Vl, G6); a TH cluster in the periventricular nucleus of the posterior tuberculum (TP/TPp, small cells, ventral to the central posterior thalamic nucleus (CP), G11) and in the posterior tuberal nucleus (PTN, G12) (Figure S5, related to Figure 4). Similar to pS6 neuronal quantification described above, we manually analyzed five coronal brain slices for each cluster, in each brain hemisphere, placing one square of 1000 μm^2 in the brain region of interest with the highest density of cells. To compare dopaminergic cell numbers between treatments, we used GLMM with a Poisson distribution followed by planned comparisons, and analyzed the eight brain areas independently, correcting the p-values with the FDR adjustment method.

Neuronal activity analysis

Generalized Linear Mixed Models (GLMM) with a Poisson regression followed by planned comparisons were used to compare adult neuronal activation ($pS6^+$ cell number) between treatments (4-6 days-old MTZ-treatment vs. untreated) and stimuli (shoal of conspecifics vs. empty). We counted pS6 positive cells in 16 brain areas (FigureS3 related to Figure3) and for each area we sampled up to 5 squares of 1000 μm^2 per brain. Because this generated pseudo-replication of brain numbers, we used the brain ID as a mixed effect in the statistical model. We analyzed the 16 brain areas independently and corrected the p-values of the planned comparisons with the FDR adjustment method (Table S3). To compare neuronal cell number activation between treatments and stimuli, we used a Generalized Linear Mixed Models (GLMM) with a Poisson distribution using the brain identification number as the mixed effect in the statistical model, followed by planned comparisons, since we target areas that are known to belong to the social decision-making network. We analyzed the 16 brain areas independently and corrected the p-values of the planned comparison with the fdr adjustment method.

Network reconstruction.

To test for functional connectivity of early MTZ-treated vs untreated brains exposed to social stimuli, we reconstructed Pearson correlation matrices using a resampling procedure, similar to the Quadratic Assignment Procedure (QAP). Instead of defining a single network, we construct the set of possible networks obtained leaving out some of the specimens' information. More precisely, consider the case of M specimens, each with an associated expression vector $x_i \in \mathbb{R}^N$, where N is the number of brain regions. For a given $m < M$, we consider all the $\binom{M}{m}$ combinations Ω_γ of m specimens and compute the corresponding functional graphs. We refer to the collection of graphs obtained in this way as a graph tower Ω_Γ, where each of the combinations can be considered as a graph layer. The advantage of this construction is that each layer in the graph tower represents a different instance of the network bootstrapping. In this way, observables computable on a single layer can be bootstrapped across multiple ones. The construction has naturally one parameter, the sampling number m, which needs to be chosen on the basis of data-driven considerations. In our experiments, robustness analysis shows that results are robust for m values between 10 and 15. To obtained sparse functional connectivity matrices, we threshold each instance following [71] at a density threshold of $\rho = 0.2$, which also corresponds to the minimum network heterogeneity across instances. After thresholding, for each treatment we average the thresholded instances to obtain a single matrix per treatment, which we use in the following analysis.

Detection of robust functional modules.

Communities were computed using the Leiden community detection method [44] on the averaged treatment matrices. To increase the robustness of the detection, for each condition, we repeat the community detection 400 times. From the 400 candidate partitions we extract the central partition as described in [45] and associate the resulting central partition to the treatment under analysis. To quantitatively characterize differences among partitions, we measure the ratio r of total edge weights within a community with that of the edges between communities. More specifically, for a partition $\mathcal{P}$ with s communities we compute the $s \times s$ matrix P, defined as

$$P_{\alpha\beta} = \sum_{i \in \alpha, j \in \beta} \omega_{ij}$$

Where $\alpha, \beta = 0, \ldots m-1$ label the modules of $\mathcal{P}$ and ω_{ij} is the edge weight between regions i and j. We then compute the ratio of average intra-community to inter-community edge weights as follows:

$$r = \frac{(m-1)\sum_{\alpha} P_{\alpha\alpha}}{2\sum_{\alpha \neq \beta} P_{\alpha\beta}} = \frac{(m-1)}{2} \frac{TrP}{|P|_1 - TrP}$$

which measures the ratio of the average weight on the diagonal of $P_{\alpha\beta}$ to the average diagonal weight. To assess significance of r values and of differences between them, we employ a permutation test based on permutating the community labels while preserving the size of the considered communities. We find that all r values are significantly different from zero, and so are also the differences in r between treatments ($p<0.01$).

Strength centrality.

As a measure of local integration, we computed also the strength centralities. The first encodes how strongly a node links to its neighbors. while the second total measures how influential a node is at the network level on the basis of its direct connections and how well connected its neighbors are. In Table XX we report the nodes ranked in decreasing order of strength (weighted degree) centrality.

Behavioral statistical analysis

Data are represented as mean ± standard error of the mean (SEM). Normality of the data was tested by D´Agostino and Pearson omnibus normality test and Shapiro-Wilk normality tests. When parametric assumptions were verified, we used parametric statistics; otherwise we used equivalent non-parametric tests.

Significance was denoted as $p < 0.05$, and p-values refer to two-tailed tests, unless otherwise noted. The use of one-tailed tests was justified by a priori directionality hypotheses in the following cases:

- Effect of MTZ treatment on OXT mRNA and NTR-mCherry transgene expression (Figure 2 and FigureS1), since in our system, we expected that MTZ would ablate the NTR-oxytocinergic expressing neurons;
- Effect of MTZ treatment (oxytocinergic ablation) on social affiliation behavior in fish expressing the NTR transgene, and thus causing OXT ablation, since OXT is well known to regulate social behaviors and thus, we expected that oxytocinergic ablation would lead to a decreased social behavior in zebrafish.

One sample *t*-tests were used to verify if social affiliation during development was statistically different from chance (0.5). We used Mann-Whitney tests to compare the effect of MTZ treatment on OXT mRNA, on the expression of the NTR-mCherry transgene, and to compare the adult social affiliation score between untreated amd MTZ-treated groups at different developmental time points (4-6 days-old, 12-14 days-old, 22-24 days-old and 90 days-old MTZ-treatment).

Because we tested eight independent cohorts for the effect of MTZ-treatment at 4-6 days-old time point (by different researchers in two different laboratories), the total sample size for this time point (n=210) was much larger than for the other time points (12-14 days-old: n=28, 22-24 days-old, n=19; adult: n=13). Taking into account all eight cohorts together, the adult social affiliation score of the 4-6 days-old MTZ-treated fish were significantly decreased from untreated siblings (p=0.0012, Mann-Whitney test, n= 112 untreated vs. 98 MTZ-treated fish). However, a Generalized Linear Model (GLM) with beta regression and planned comparisons, which was used to compare the effect of MTZ treatment on adult social affiliation score of the eight different cohorts (FigureS1 related to Figure2), revealed not only an effect of the MTZ treatment (F_1=9.486, p=0.0021) but also variation among cohorts (F_7=2.719, p=0.0081). We therefore performed a Monte Carlo simulation for a sample size of 30 individuals, 15 individuals from each group (untreated and 4-6 days-old MTZ treated) with 1000 iterations. This simulation, ensured a more comparable sample size for the 4-6 days-old time point treatment relative to other time-point treatments. . Moreover, it ensured a more representative sample than each cohort independently or the total eight-cohort population. We obtained a Monte Carlo p-value of p<0.001 (Figure 2E), which means that there was a significantly higher number of simulations in which the social affiliation score of the untreated group was greater than

the social affiliation score of the MTZ-treated group, as compared to the number of simulations with the inverse trend, for a sample size of 15 individuals, across all eight cohorts. It was calculated as the mean social affiliation score of the 1000 iterations for untreated fish divided by the mean scores of the 1000 iterations for treated fish divided by 1000.

To determine whether the difference in social affiliation score between untreated and 4-6 days-old MTZ-treated fish was due to OXT ablation and not movement impairments caused by MTZ, we used a Linear Model (LM) to compare the total distance moved (square root transformed) of both groups in the eight independent cohorts. Both GLM with beta regression on adult social affiliation score and LM on total distance moved (square root transformed) were also applied to different control cohort fish not expressing NTR transgene (FigureS2-Related to Figure2).

LM was performed to assess the effect of 4-6 days-old MTZ-treatment in total TH counts of three distinct TH clusters in 8 days-old larvae (Figure4 and Table S5). The effect of 4-6 days-old MTZ treatment on adult dopaminergic system was also assessed with a GLMM with a Poisson regression followed by planned comparisons, comparing the number of TH-positive cells sampled in five squares of 1000 μm^2 per TH cluster in 8 different adult brain TH clusters. All eight areas were analyzed independently and p-values of the planned comparisons were corrected with the fdr adjustment method (Figure4 and Table S6).

Graphical representations of the data were performed in GraphPad Prism 6.0c software. Shapiro-Wilk normality test, one-sample *t*-test and *t*-tests were performed in GraphPad Prism, and the remaining tests were performed in R programming software, version 3.6.3 (R Core Team 2020)[72] with the following packages: lme4[73] and afex[74] (for GLMM with Poisson regression), betareg (for GLMM with beta regression), emmeans (for planned comparisons)[75], and the base R package (for LM regression and Monte Carlo simulations)[72].

List of Supplementary tables

Table S1. Effect of 4-6 days-old MTZ treatment on adult social affiliation and total distance moved in eight independent cohorts of zebrafish expressing the oxt:ntr transgene.

Table S2. Effect of 4-6 days-old MTZ treatment on adult social affiliation and total distance moved in control zebrafish not expressing the transgene NTR.

Table S3. Effect of 4-6 days-old MTZ-treatment in TH cell clusters of larvae zebrafish brain.

Table S4. Effect of 4-6 days-old MTZ-treatment in TH cell clusters of adult zebrafish brain.

Table S5. Effect of 4-6 days-old MTZ treatment on adult neuronal activation.

Table S6. Rank of node strength centralities.

Table S1. Effects of 4-6 days-old MTZ treatment in adult social affiliation and total distance moved on eight independent experimental cohorts tested

Social affiliation behavior (GLM)

	d.f.1	d.f.2	F.ratio	p.value
Cohort	7	inf	2.719	0.0081**
Treatment	1	inf	9.486	0.00105**
Cohort:Treatment	7	inf	1.388	0.2053

Total Distance moved (LM)

	Df	Sum Sq	Mean Sq	F value	Pr(>F)
Cohort	7	17444	2492.03	15.2007	8.342e-16***
Treatment	1	30	30.22	0.1843	0.6681
Cohort: Treatment	7	838	119.67	0.7299	0.6468
Residuals	195	31969	163.94		

Summary of results of the GLM (Generalized Linear Model) with beta regression and LM (Linear Model) models to analyse the effects of early (4-6 days-old) MTZ-treatment on adult social affiliation and total distance moved on eight independent experimental cohorts expressing the NTR transgene. A one-tailed p-value was considered for the effect of MTZ-treatment on social affiliation behaviour because of our a priori directionality hypothesis (see Methods/Statistic section).

Table S.2. Effects of 4-6 days-old MTZ-treatment in adult social affiliation and total distance moved on control fish not expressing the NTR transgene

Social affiliation behavior (GLM)

	d.f.1	d.f.2	F.ratio	p.value
Cohort	3	inf	7.249	0.0001***
Treatment	1	inf	1.241	0.2653
Cohort:Treatment	3	inf	1.271	0.2822

Total Distance moved (LM)

	Df	Sum Sq	Mean Sq	F value	Pr(>F)
Cohort	3	15614.2	5204.7	58.5513	<2e-16***
Treatment	1	183.3	183.3	2.0615	0.1536
Cohort: Treatment	3	352.1	117.4	1.3203	0.2710
Residuals	121	10755.9	88.9		

Summary of results of the GLM with beta regression and LM models to analyse the effects of early (4-6 days-old) MTZ-treatment on adult social affiliation and total distance moved on control fish not expressing the NTR transgene.

Table S3. Effect of 4-6 days-old MTZ-treatment in TH cell clusters of larvae zebrafish brain.
Three independent brain areas were analyzed. Linear model with post-hoc tests comparing the treatment (early MTZ-treated vs. untreated) were performed.

BA	Treat1	Treat2	estim	SE	z.ratio	*p*.value
Subpallium	Untreated	MTZ-Treated	-2.889	2.622	-1.102	0.278
PrT	Untreated	MTZ-Treated	-8.278	2.994	-2.764	0.009 **
PT Large cells	Untreated	MTZ-Treated	-1.722	0.566	-3.042	0.0045**

BA, Brain area; *Treat*, Treatment; *estim*, estimate; *PrT,* Pretectum; *TP*, Posterior Tuberculum.

Table S4. Effect of 4-6 days-old MTZ-treatment in TH cell clusters of adult zebrafish brain. Eight independent brain areas were analyzed. GLMM with a Poisson regression and planned comparisons (early MTZ-Treated vs. Untreated) was performed. *p*-values from planned comparisons were corrected with false discovery rate (fdr) adjustment method.

BA	Treat1	Treat2	estim	SE	z.ratio	*p*.value. indep. GLMM	*p*.value. indep. GLMM. fdr correction
Subpallium (G2)	Untreated	MTZ-Treated	-0.031	0.0562	-0.552	0.5813	0.6643
PPa (G3)	Untreated	MTZ-Treated	0.185	0.175	1.058	0.2901	0.3868
PPa (G4)	Untreated	MTZ-Treated	0.0611	0.0533	1.147	0.2513	0.3868
PPp (G5)	Untreated	MTZ-Treated	0.12	0.0747	1.603	0.1090	0.218
Vm + Vl (G6)	Untreated	MTZ-Treated	0.0143	0.0755	0.189	0.8502	0.8502
PrT (G7)	Untreated	MTZ-Treated	0.201	0.0598	3.364	0.0008	0.0048**
TP (G11)	Untreated	MTZ-Treated	0.188	0.0724	2.597	0.0094	0.0251*
PTN (G12)	Untreated	MTZ-Treated	0.19	0.0586	3.239	0.0012	0.0048**

BA, Brain area; *Treat*, Treatment; *estim*, estimate; *GLMM*, Generalized Linear Mixed Models; *fdr*, false discovery rate, *PPa*, anterior part of the parvocellular preoptic nucleus; *PPp*, posterior part of the Parvocellular preoptic nucleus; *Vm*, ventromedial thalamic nucleus; *Vl*, ventrolateral thalamic nucleus; *PrT*, Pretectum nucleus; *TP*, Posterior tuberculum nucleus; *PTN*, Posterior Tuberal nucleus.

Table S5. Effect of 4-6 days-old MHZ treatment on adult neuronal activation. Neuronal activation measured by pS6 immunostaining. Sixteen (16) independently brain areas were analyzed. GLMM with a Poisson regression and planned comparisons were performed. *p*-values of the planned comparisons were corrected with false discovery rate (fdr) adjustment method (significant values in red).

BA1	Stim1	Treat1	BA2	Stim2	Treat2	estim	SE	z.ratio	*p*.value. indep. GLMM	*p*.value. indep. GLMM. fdr correction
Dd	EMPTY	CTR	Dd	SHOAL	CTR	-0.2076	0.125	-1.655	0.0978	0.4084
Dd	EMPTY	ABLAT	Dd	EMPTY	CTR	-0.2057	0.147	-1.399	0.1618	0.523687
Dd	SHOAL	ABLAT	Dd	SHOAL	CTR	-0.0078	0.118	-0.066	0.9477	0.9683302
Dd	EMPTY	ABLAT	Dd	SHOAL	ABLAT	-0.0096	0.138	-0.069	0.9448	0.9683302
DL	EMPTY	CTR	DL	SHOAL	CTR	-0.096	0.0948	-1.013	0.311	0.7052
DL	EMPTY	ABLAT	DL	EMPTY	CTR	-0.1449	0.1067	-1.359	0.1743	0.523687
DL	SHOAL	ABLAT	DL	SHOAL	CTR	-0.1496	0.0831	-1.8	0.0718	0.4084
DL	EMPTY	ABLAT	DL	SHOAL	ABLAT	-0.1007	0.0964	-1.044	0.2964	0.7025778
DM	EMPTY	CTR	DM	SHOAL	CTR	-0.0206	0.118	-0.174	0.8617	0.9347254
DM	EMPTY	ABLAT	DM	EMPTY	CTR	-0.0238	0.135	-0.177	0.8598	0.9347254
DM	SHOAL	ABLAT	DM	SHOAL	CTR	-0.1401	0.105	-1.332	0.1827	0.523687
DM	EMPTY	ABLAT	DM	SHOAL	ABLAT	-0.1369	0.124	-1.107	0.2683	0.6604308
PPA	**EMPTY**	**CTR**	**PPA**	**SHOAL**	**CTR**	**-0.2858**	**0.0899**	**-3.18**	**0.0015**	**0.024**
PPA	**EMPTY**	**ABLAT**	**PPA**	**EMPTY**	**CTR**	**0.3415**	**0.1018**	**3.356**	**0.0008**	**0.024**
PPA	SHOAL	ABLAT	PPA	SHOAL	CTR	0.017	0.0793	0.215	0.83	0.9347254
PPA	EMPTY	ABLAT	PPA	SHOAL	ABLAT	0.0387	0.0926	0.418	0.6761	0.8830694
PPp	EMPTY	CTR	PPp	SHOAL	CTR	-0.2579	0.116	-2.229	0.0258	0.2638222
PPp	EMPTY	ABLAT	PPp	EMPTY	CTR	-0.1959	0.129	-1.521	0.1284	0.4833882
PPp	SHOAL	ABLAT	PPp	SHOAL	CTR	-0.0306	0.103	-0.297	0.7663	0.9082074
PPp	EMPTY	ABLAT	PPp	SHOAL	ABLAT	-0.0926	0.117	-0.789	0.4302	0.795241
VC_a	EMPTY	CTR	VC_a	SHOAL	CTR	0.0668	0.141	0.474	0.6358	0.8830694
VC_a	EMPTY	ABLAT	VC_a	EMPTY	CTR	-0.3189	0.153	-2.085	0.0371	0.2638222
VC_a	SHOAL	ABLAT	VC_a	SHOAL	CTR	-0.2749	0.132	-2.085	0.0371	0.2638222
VC_a	EMPTY	ABLAT	VC_a	SHOAL	ABLAT	0.1107	0.144	0.767	0.4433	0.795241
VC_p	EMPTY	CTR	VC_p	SHOAL	CTR	-0.0203	0.133	-0.153	0.8786	0.9371733
VC_p	EMPTY	ABLAT	VC_p	EMPTY	CTR	-0.1035	0.146	-0.708	0.4789	0.795241
VC_p	SHOAL	ABLAT	VC_p	SHOAL	CTR	-0.0401	0.116	-0.347	0.7285	0.9082074
VC_p	EMPTY	ABLAT	VC_p	SHOAL	ABLAT	0.0431	0.131	0.33	0.7417	0.9082074
VD_a	EMPTY	CTR	VD_a	SHOAL	CTR	-0.2073	0.161	-1.287	0.1981	0.5282667
VD_a	EMPTY	ABLAT	VD_a	EMPTY	CTR	-0.1121	0.17	-0.659	0.5102	0.81632
VD_a	SHOAL	ABLAT	VD_a	SHOAL	CTR	0.0089	0.152	0.059	0.9532	0.9683302
VD_a	EMPTY	ABLAT	VD_a	SHOAL	ABLAT	-0.0862	0.162	-0.533	0.5942	0.8830694
VD_m	EMPTY	CTR	VD_m	SHOAL	CTR	0.0482	0.115	0.419	0.6749	0.8830694
VD_m	EMPTY	ABLAT	VD_m	EMPTY	CTR	-0.2684	0.125	-2.147	0.0318	0.2638222
VD_m	SHOAL	ABLAT	VD_m	SHOAL	CTR	-0.0759	0.109	-0.699	0.4846	0.795241
VD_m	EMPTY	ABLAT	VD_m	SHOAL	ABLAT	0.2407	0.119	2.016	0.0438	0.28032
VD_p	EMPTY	CTR	VD_p	SHOAL	CTR	0.112	0.114	0.985	0.3247	0.7052
VD_p	EMPTY	ABLAT	VD_p	EMPTY	CTR	-0.169	0.125	-1.355	0.1754	0.523687
VD_p	SHOAL	ABLAT	VD_p	SHOAL	CTR	-0.173	0.104	-1.661	0.0968	0.4084
VD_p	EMPTY	ABLAT	VD_p	SHOAL	ABLAT	0.108	0.116	0.932	0.3513	0.7052
VL	EMPTY	CTR	VL	SHOAL	CTR	0.00959	0.328	0.029	0.9767	0.9767
VL	EMPTY	ABLAT	VL	EMPTY	CTR	0.06954	0.365	0.19	0.8491	0.9347254

VL	SHOAL	ABLAT	VL	SHOAL	CTR	0.14089	0.309	0.455	0.6489	0.8830694
VL	EMPTY	ABLAT	VL	SHOAL	ABLAT	0.08094	0.349	0.232	0.8165	0.9347254
VM	EMPTY	CTR	VM	SHOAL	CTR	-0.3257	0.265	-1.231	0.2184	0.559104
VM	EMPTY	ABLAT	VM	EMPTY	CTR	0.1426	0.299	0.476	0.6339	0.8830694
VM	SHOAL	ABLAT	VM	SHOAL	CTR	0.3621	0.248	1.461	0.144	0.512
VM	EMPTY	ABLAT	VM	SHOAL	ABLAT	-0.1062	0.285	-0.373	0.7089	0.907392
VP	EMPTY	CTR	VP	SHOAL	CTR	-0.2041	0.123	-1.663	0.0963	0.4084
VP	EMPTY	ABLAT	VP	EMPTY	CTR	-0.1158	0.145	-0.8	0.4234	0.795241
VP	SHOAL	ABLAT	VP	SHOAL	CTR	0.1484	0.113	1.316	0.1882	0.523687
VP	EMPTY	ABLAT	VP	SHOAL	ABLAT	0.06	0.135	0.446	0.6559	0.8830694
VS	EMPTY	CTR	VS	SHOAL	CTR	-0.3116	0.117	-2.664	0.0077	0.09856
VS	EMPTY	ABLAT	VS	EMPTY	CTR	-0.1251	0.133	-0.938	0.3483	0.7052
VS	SHOAL	ABLAT	VS	SHOAL	CTR	0.0968	0.104	0.93	0.3526	0.7052
VS	EMPTY	ABLAT	VS	SHOAL	ABLAT	-0.0897	0.122	-0.734	0.4628	0.795241
VV_a	**EMPTY**	**CTR**	**VV_a**	**SHOAL**	**CTR**	**0.6076**	**0.19**	**3.193**	**0.0014**	**0.024**
VV_a	EMPTY	ABLAT	VV_a	EMPTY	CTR	0.0626	0.205	0.305	0.7606	0.9082074
VV_a	**SHOAL**	**ABLAT**	**VV_a**	**SHOAL**	**CTR**	**-0.6333**	**0.181**	**-3.504**	**0.0005**	**0.024**
VV_a	EMPTY	ABLAT	VV_a	SHOAL	ABLAT	-0.0883	0.197	-0.449	0.6537	0.8830694
VV_p	EMPTY	CTR	VV_p	SHOAL	CTR	0.0579	0.114	0.509	0.611	0.8830694
VV_p	EMPTY	ABLAT	VV_p	EMPTY	CTR	-0.2034	0.124	-1.635	0.1021	0.4084
VV_p	SHOAL	ABLAT	VV_p	SHOAL	CTR	-0.1748	0.104	-1.687	0.0915	0.4084
VV_p	EMPTY	ABLAT	VV_p	SHOAL	ABLAT	0.0865	0.115	0.751	0.4529	0.795241

BA1, Brain area 1; *BA2*, Brain area 2; *Stim*, stimulus; *Treat*, Treatment; *estim*, estimate; *indep*., independent, *GLMM*, Generalized Linear Mixed Models; *fdr*, false discovery rate, *CTR*, untreated fish; *ABLT*, early MTZ-treated fish; *Vv_a*, anterior part of the ventral nucleus of the ventral telencephalic area (V); *Vv_p*, posterior part of the ventral nucleus of the ventral telencephalic area (V); *Vd_a*, anterior part of the dorsal nucleus of V; *Vd_m*, medial part of the dorsal nucleus of V; *Vd_p*, posterior part of the dorsal nucleus of V; *Vc_a*, anterior part of the central nucleus of V; *Vc_p*, posterior part of the central nucleus of V; *Dm*, medial zone of the dorsal telencephalic area (D); *Dl*, lateral zone of the dorsal telencephalic area (D); *Dd*, dorsal zone of the dorsal telencephalic area (D); *Vs*, supracommissural nucleus of V; *Vp*, postcommissural nucleus of V; *Ppa*, anterior part of the parvocellular preoptic nucleus; *Ppp*, posterior part of the parvocellular preoptic nucleus; *VM*, ventromedial thalamic nucleus; *VL*, ventrolateral thalamic nucleus.

Table S6: Rank of node strength centralities of adult treated vs untreated zebrafish exposed to a conspecific shoal or to empty compartments.

Rank	AE	AS	CE	CS
1	DM	VD_a	VD_p	VV_p
2	DL	VL	VC_p	DM
3	VS	VV_a	VV_a	Dd
4	VP	VM	VV_p	PPA
5	VV_p	VV_p	Dd	VD_p
6	VD_m	VP	VD_a	VC_p
7	VL	VD_m	VC_a	VC_a
8	Dd	VS	VD_m	VS
9	PPp	VC_p	PPp	VP
10	VD_p	VD_p	VL	DL
11	VM	PPA	VM	VV_a
12	VC_p	PPp	DL	VD_m
13	VC_a	DL	DM	VM
14	VD_a	VC_a	VP	VD_a
15	VV_a	Dd	PPA	PPp
16	PPA	DM	VS	VL

AE, early-MTZ treated fish exposed to empty compartment; *AS*, early MTZ-treated fish exposed to shoal; CE, untreated fish exposed to empty compartment; CS, untreated fish exposed to shoal; *Vv_a*, anterior part of the ventral nucleus of the ventral telencephalic area (V); *Vv_p*, posterior part of the ventral nucleus of the ventral telencephalic area (V); *Vd_a*, anterior part of the dorsal nucleus of V; *Vd_m*, medial part of the dorsal nucleus of V; *Vd_p*, posterior part of the dorsal nucleus of V; *Vc_a*, anterior part of the central nucleus of V; *Vc_p*, posterior part of the central nucleus of V; *Dm*, medial zone of the dorsal telencephalic area (D); *Dl*, lateral zone of the dorsal telencephalic area (D); *Dd*, dorsal zone of the dorsal telencephalic area (D); *Vs*, supracommissural nucleus of V; *Vp*, postcommissural nucleus of V; *Ppa*, anterior part of the parvocellular preoptic nucleus; *Ppp*, posterior part of the parvocellular preoptic nucleus; *VM*, ventromedial thalamic nucleus; *VL*, ventrolateral thalamic nucleus;